

Interpolation-Based QR Decomposition in MIMO-OFDM Systems^{☆,☆☆}

Davide Cescato^a, Helmut Bölcskei^{*,a}

^a*Communication Technology Laboratory, ETH Zurich, 8092 Zurich, Switzerland*

Abstract

Detection algorithms for multiple-input multiple-output (MIMO) wireless systems based on orthogonal frequency-division multiplexing (OFDM) typically require the computation of a QR decomposition for each of the data-carrying OFDM tones. The resulting computational complexity will, in general, be significant, as the number of data-carrying tones ranges from 48 (as in the IEEE 802.11a/g standards) to 1728 (as in the IEEE 802.16e standard). Motivated by the fact that the channel matrices arising in MIMO-OFDM systems are highly oversampled polynomial matrices, we formulate interpolation-based QR decomposition algorithms. An in-depth complexity analysis, based on a metric relevant for very large scale integration (VLSI) implementations, shows that the proposed algorithms, for sufficiently high number of data-carrying tones and sufficiently small channel order, provably exhibit significantly smaller complexity than brute-force per-tone QR decomposition.

Key words: Interpolation, polynomial matrices, multiple-input multiple-output (MIMO) systems, orthogonal frequency-division multiplexing (OFDM), QR decomposition, successive cancelation, sphere decoding, very large scale integration (VLSI).

1. Introduction and Outline

The use of orthogonal frequency-division multiplexing (OFDM) drastically reduces data detection complexity in wideband multiple-input multiple-output (MIMO) wireless systems by decoupling a frequency-selective fading MIMO channel into a set of flat-fading MIMO channels. Nevertheless, MIMO-OFDM detectors still pose significant challenges in terms of computational complexity, as processing has to be performed on a per-tone basis with the number of data-carrying tones ranging from 48 (as in the IEEE 802.11a/g wireless local area network standards) to 1728 (as in the IEEE 802.16 wireless metropolitan area network standard).

[☆]This work was supported in part by the Swiss National Science Foundation under grant No. 200021-100025/1.

^{☆☆}Parts of this paper were presented at the Sixth IEEE Workshop on Signal Processing Advances in Wireless Communications (SPAWC), New York, NY, June 2005.

*Corresponding author. Tel.: +41 44 632 3433, fax: +41 44 632 1209.

Email addresses: dcescato@nari.ee.ethz.ch (Davide Cescato), boelcskei@nari.ee.ethz.ch (Helmut Bölcskei)

Preprint submitted to Elsevier

November 1, 2018

Specifically, in the setting of coherent MIMO-OFDM detection, for which the receiver is assumed to have perfect channel knowledge, linear MIMO-OFDM detectors [13] require matrix inversion, whereas successive cancellation receivers [21] and sphere decoders [5, 17] require QR decomposition, in all cases on each of the data-carrying OFDM tones. The corresponding computations, termed as *preprocessing* in the following, have to be performed at the rate of change of the channel which, depending on the propagation environment, is typically much lower than the rate at which the transmission of actual data symbols takes place. Nevertheless, as payload data received during the preprocessing phase must be stored in a dedicated buffer, preprocessing represents a major bottleneck in terms of the size of this buffer and the resulting detection latency [14].

In a very large scale integration (VLSI) implementation, the straightforward approach to reducing the preprocessing latency is to employ parallel processing over multiple matrix inversion or QR decomposition units, which, however, comes at the cost of increased silicon area. In [1], the problem of reducing preprocessing complexity in linear MIMO-OFDM receivers is addressed on an algorithmic level by formulating efficient interpolation-based algorithms for matrix inversion that take the polynomial nature of the MIMO-OFDM channel matrix explicitly into account. Specifically, the algorithms proposed in [1] exploit the fact that the channel matrices arising in MIMO-OFDM systems are polynomial matrices that are highly oversampled on the unit circle. The goal of the present paper is to devise computationally efficient interpolation-based algorithms for QR decomposition in MIMO-OFDM systems. Although throughout the paper we focus on QR decomposition in the context of coherent MIMO-OFDM detectors, our results also apply to transmit precoding schemes for MIMO-OFDM (under the assumption of perfect channel knowledge at the transmitter) requiring per-tone QR decomposition [20].

Contributions. Our contributions can be summarized as follows:

- We present a new result on the QR decomposition of Laurent polynomial (LP) matrices, based on which interpolation-based algorithms for QR decomposition in MIMO-OFDM systems are formulated.
- Using a computational complexity metric relevant for VLSI implementations, we demonstrate that, for a wide range of system parameters, the proposed interpolation-based algorithms exhibit significantly smaller complexity than brute-force per-tone QR decomposition.
- We present different strategies for efficient LP interpolation that take the specific structure of the problem at hand into account and thereby enable (often significant) computational complexity savings of interpolation-based QR decomposition.
- We provide a numerical analysis of the trade-off between the computational complexity of the interpolation-based QR decomposition algorithms presented and the performance of corresponding MIMO-OFDM detectors.

Outline of the paper. In Section 2, we present the mathematical preliminaries needed in the rest of the paper. In Section 3, we briefly review the use of QR decomposition in MIMO-OFDM receivers, and we formulate the problem statement. In Section 4, we present our main technical result on the QR decomposition of LP matrices. This result is then used in Section 5 to formulate interpolation-based algorithms for QR decomposition of MIMO-OFDM channel matrices. Section 6 contains an in-depth computational complexity analysis of the proposed algorithms. In Section 7, we describe the application of the new approach to the QR decomposition of the augmented MIMO-OFDM channel matrices arising in the context of minimum mean-square error (MMSE) receivers. In Section 8, we discuss methods for LP interpolation that exploit the specific structure of the problem at hand and exhibit low VLSI implementation complexity. Section 9 contains numerical results on the computational complexity of the proposed interpolation-based QR decomposition algorithms along with a discussion of the trade-off between algorithm complexity and MIMO-OFDM receiver performance. We conclude in Section 10.

2. Mathematical Preliminaries

2.1. Notation

$\mathbb{C}^{P \times M}$ denotes the set of complex-valued $P \times M$ matrices. $\mathcal{U} \triangleq \{s \in \mathbb{C} : |s| = 1\}$ indicates the unit circle. \emptyset is the empty set. $|\mathcal{A}|$ stands for the cardinality of the set \mathcal{A} . mod is the modulo operator. All logarithms are to the base 2. $\mathbb{E}[\cdot]$ denotes the expectation operator. $\mathcal{CN}(\mathbf{0}, \mathbf{K})$ stands for the multivariate, circularly-symmetric complex Gaussian distribution with covariance matrix \mathbf{K} . Throughout the paper, we use the following conventions. First, if $k_2 < k_1$, $\sum_{k=k_1}^{k_2} \alpha_k = 0$, regardless of α_k . Second, sequences of integers of the form $k_1, k_1 + \Delta, \dots, k_2$, with $\Delta > 0$, simplify to the sequence k_1, k_2 if $k_2 = k_1 + \Delta$, to the single value k_1 if $k_2 = k_1$, and to the empty sequence if $k_2 < k_1$.

\mathbf{A}^* , \mathbf{A}^T , \mathbf{A}^H , \mathbf{A}^\dagger , $\text{rank}(\mathbf{A})$, and $\text{ran}(\mathbf{A})$ denote the entrywise conjugate, the transpose, the conjugate transpose, the pseudoinverse, the rank, and the range space, respectively, of the matrix \mathbf{A} . $[\mathbf{A}]_{p,m}$ indicates the entry in the p th row and m th column of \mathbf{A} . $\mathbf{A}^{p_1:p_2}$ and $\mathbf{A}_{m_1:m_2}$ stand for the submatrix given by the rows $p_1, p_1 + 1, \dots, p_2$ of \mathbf{A} and the submatrix given by the columns $m_1, m_1 + 1, \dots, m_2$ of \mathbf{A} , respectively. Furthermore, we set $\mathbf{A}_{m_1:m_2}^{p_1:p_2} \triangleq (\mathbf{A}_{m_1:m_2})^{p_1:p_2}$ and $\mathbf{A}_{m_1:m_2}^H \triangleq (\mathbf{A}_{m_1:m_2})^H$. A $P \times M$ matrix \mathbf{A} is said to be upper triangular if all entries below its main diagonal $\{[\mathbf{A}]_{k,k} : k = 1, 2, \dots, \min(P, M)\}$ are equal to zero. $\det(\mathbf{A})$ and $\text{adj}(\mathbf{A})$ denote the determinant and the adjoint of a square matrix \mathbf{A} , respectively. $\text{diag}(a_1, a_2, \dots, a_M)$ indicates the $M \times M$ diagonal matrix with the scalar a_m as its m th main diagonal element. \mathbf{I}_M stands for the $M \times M$ identity matrix, $\mathbf{0}$ denotes the all-zeros matrix of appropriate size, and \mathbf{W}_M is the $M \times M$ discrete Fourier transform matrix, given by $[\mathbf{W}_M]_{p+1,q+1} = e^{-j2\pi pq/M}$ ($p, q = 0, 1, \dots, M-1$). Finally, orthogonality and norm of complex-valued vectors $\mathbf{a}_1, \mathbf{a}_2$ are induced by the inner product $\mathbf{a}_1^H \mathbf{a}_2$.

2.2. QR Decomposition

Throughout this section, we consider a matrix $\mathbf{A} = [\mathbf{a}_1 \ \mathbf{a}_2 \ \cdots \ \mathbf{a}_M] \in \mathbb{C}^{P \times M}$ with $P \geq M$, where \mathbf{a}_k denotes the k th column of \mathbf{A} ($k = 1, 2, \dots, M$). In the remainder of the paper, the term QR decomposition refers to the following:

Definition 1. We call any factorization $\mathbf{A} = \mathbf{Q}\mathbf{R}$, for which the matrices $\mathbf{Q} \in \mathbb{C}^{P \times M}$ and $\mathbf{R} \in \mathbb{C}^{M \times M}$ satisfy the following conditions, a *QR decomposition* of \mathbf{A} with *QR factors* \mathbf{Q} and \mathbf{R} :

1. the nonzero columns of \mathbf{Q} are orthonormal
2. \mathbf{R} is upper triangular with real-valued nonnegative entries on its main diagonal
3. $\mathbf{R} = \mathbf{Q}^H \mathbf{A}$

Practical algorithms for QR decomposition are either based on Gram-Schmidt (GS) orthonormalization or on unitary transformations (UT). We next briefly review both classes of algorithms. GS-based QR decomposition is summarized as follows. For $k = 1, 2, \dots, M$, the k th column of \mathbf{Q} , denoted by \mathbf{q}_k , is determined by

$$\mathbf{y}_k \triangleq \mathbf{a}_k - \sum_{i=1}^{k-1} \mathbf{q}_i^H \mathbf{a}_k \mathbf{q}_i \quad (1)$$

with

$$\mathbf{q}_k = \begin{cases} \frac{\mathbf{y}_k}{\sqrt{\mathbf{y}_k^H \mathbf{y}_k}}, & \mathbf{y}_k \neq \mathbf{0} \\ \mathbf{0}, & \mathbf{y}_k = \mathbf{0} \end{cases} \quad (2)$$

whereas the k th row of \mathbf{R} , denoted by \mathbf{r}_k^T , is given by

$$\mathbf{r}_k^T = \mathbf{q}_k^H \mathbf{A}. \quad (3)$$

UT-based QR decomposition of \mathbf{A} is performed by left-multiplying \mathbf{A} by the product $\Theta_U \cdots \Theta_2 \Theta_1$ of $P \times P$ unitary matrices Θ_u , where the sequence of matrices $\Theta_1, \Theta_2, \dots, \Theta_U$ and the parameter U are not unique and are chosen such that the $P \times M$ matrix $\Theta_U \cdots \Theta_2 \Theta_1 \mathbf{A}$ is upper triangular with nonnegative real-valued entries on its main diagonal. The matrices Θ_u are typically either Givens rotation matrices [6] or Householder reflection matrices [6]. With $\mathbf{R} \triangleq (\Theta_U \cdots \Theta_2 \Theta_1 \mathbf{A})^{1,M}$ and $\mathbf{Q} \triangleq ((\Theta_U \cdots \Theta_2 \Theta_1)^H)_{1,M}$, we obtain that $\mathbf{Q}^H \mathbf{A} = \mathbf{R}$ and, since $\Theta_U \cdots \Theta_2 \Theta_1$ is unitary, that $\mathbf{Q}^H \mathbf{Q} = \mathbf{I}_M$. Therefore, \mathbf{Q} and \mathbf{R} are QR factors of \mathbf{A} . For $P > M$, we note that the $P \times (P - M)$ matrix $\mathbf{Q}^\perp \triangleq ((\Theta_U \cdots \Theta_2 \Theta_1)^H)_{M+1,P}$ satisfies $(\mathbf{Q}^\perp)^H \mathbf{Q}^\perp = \mathbf{I}_{P-M}$ and $\mathbf{Q}^H \mathbf{Q}^\perp = \mathbf{0}$. In practice, UT-based QR decomposition of \mathbf{A} can be performed as follows [6, 3]. A $P \times M$ matrix \mathbf{X} and a $P \times P$ matrix \mathbf{Y} are initialized as $\mathbf{X} \leftarrow \mathbf{A}$ and $\mathbf{Y} \leftarrow \mathbf{I}_P$, respectively, and the counter u is set to zero. Then, u is incremented by one, and \mathbf{X} and \mathbf{Y} are updated according to $\mathbf{X} \leftarrow \Theta_u \mathbf{X}$ and $\mathbf{Y} \leftarrow \Theta_u \mathbf{Y}$, for an appropriately chosen matrix Θ_u . This update step is repeated until \mathbf{X}

becomes upper-triangular with nonnegative real-valued entries on its main diagonal. The parameter U is obtained as the final value of the counter u , and the final values of \mathbf{X} and \mathbf{Y} are

$$\mathbf{X} = \begin{bmatrix} \mathbf{R} \\ \mathbf{0} \end{bmatrix}, \mathbf{Y} = \begin{bmatrix} \mathbf{Q}^H \\ (\mathbf{Q}^\perp)^H \end{bmatrix}.$$

Since the u th update step can be represented as $[\mathbf{X} \ \mathbf{Y}] \leftarrow \Theta_u[\mathbf{X} \ \mathbf{Y}]$, we can describe UT-based QR decomposition of \mathbf{A} by means of the formal relation

$$\Theta_U \cdots \Theta_2 \Theta_1 [\mathbf{A} \ \mathbf{I}_P] = \begin{bmatrix} \mathbf{R} & \mathbf{Q}^H \\ \mathbf{0} & (\mathbf{Q}^\perp)^H \end{bmatrix} \quad (4)$$

which, from now on, will be called *standard form* of UT-based QR decomposition, and will be needed in Section 7.1 in the context of regularized QR decomposition. The standard form (4) shows that for $P > M$, UT-based QR decomposition yields the $(P - M) \times P$ matrix $(\mathbf{Q}^\perp)^H$ as a by-product. For $P = M$, the right-hand side (RHS) of (4) reduces to $[\mathbf{R} \ \mathbf{Q}^H]$.

We note that since $\mathbf{y}_1 = \mathbf{0}$ is equivalent to $\mathbf{a}_1 = \mathbf{0}$ and $\mathbf{y}_k = \mathbf{0}$ is equivalent to $\text{rank}(\mathbf{A}_{1,k-1}) = \text{rank}(\mathbf{A}_{1,k})$ ($k = 2, 3, \dots, M$) [9], GS-based QR decomposition sets $M - \text{rank}(\mathbf{A})$ columns of \mathbf{Q} and the corresponding $M - \text{rank}(\mathbf{A})$ rows of \mathbf{R} to zero. In contrast, UT-based QR decomposition yields a matrix \mathbf{Q} such that $\mathbf{Q}^H \mathbf{Q} = \mathbf{I}_M$, regardless of the value of $\text{rank}(\mathbf{A})$, and sets $M - \text{rank}(\mathbf{A})$ entries on the main diagonal of \mathbf{R} to zero [6]. Hence, for $\text{rank}(\mathbf{A}) < M$, different QR decomposition algorithms will in general produce different QR factors.

Proposition 2. *If $\text{rank}(\mathbf{A}) = M$, Conditions 1 and 2 of Definition 1 simplify, respectively, to*

1. $\mathbf{Q}^H \mathbf{Q} = \mathbf{I}_M$
2. \mathbf{R} is upper triangular with $[\mathbf{R}]_{k,k} > 0, k = 1, 2, \dots, M$

whereas Condition 3 is redundant. Moreover, \mathbf{A} has unique QR factors.

Proof. Since $\mathbf{A} = \mathbf{QR}$ implies $\text{rank}(\mathbf{A}) \leq \min\{\text{rank}(\mathbf{Q}), \text{rank}(\mathbf{R})\}$, it follows from $\text{rank}(\mathbf{A}) = M$ that $\text{rank}(\mathbf{Q}) = \text{rank}(\mathbf{R}) = M$. Now, $\text{rank}(\mathbf{Q}) = M$ implies that the $P \times M$ matrix \mathbf{Q} can not contain all-zero columns, and hence Condition 1 is equivalent to $\mathbf{Q}^H \mathbf{Q} = \mathbf{I}_M$. Moreover, $\text{rank}(\mathbf{R}) = M$ implies $\det(\mathbf{R}) \neq 0$ and, since \mathbf{R} is upper triangular, we have $\det(\mathbf{R}) = \prod_{k=1}^M [\mathbf{R}]_{k,k}$. Hence, Condition 2 becomes $[\mathbf{R}]_{k,k} > 0, k = 1, 2, \dots, M$. Condition 3 is redundant since $\mathbf{A} = \mathbf{QR}$, together with $\mathbf{Q}^H \mathbf{Q} = \mathbf{I}_M$, implies $\mathbf{Q}^H \mathbf{A} = \mathbf{R}$. The uniqueness of \mathbf{Q} and \mathbf{R} is proven in [9], Sec. 2.6. \square

We conclude by noting that for full-rank \mathbf{A} , the uniqueness of \mathbf{Q} and \mathbf{R} implies that $\mathbf{A} = \mathbf{QR}$ can be called *the* QR decomposition of \mathbf{A} with *the* QR factors \mathbf{Q} and \mathbf{R} .

2.3. Laurent Polynomials and Interpolation

In the remainder of the paper, the term *interpolation* indicates LP interpolation, as presented in this section. Interpolation is a central component of the algorithms for efficient QR decomposition of polynomial matrices presented in Sections 5 and 7. In the following, we review basic results on interpolation and establish the corresponding notation. In Section 8, we will present various strategies for computationally efficient interpolation tailored to the problem at hand.

Definition 3. Given a matrix-valued function $\mathbf{A} : \mathcal{U} \rightarrow \mathbb{C}^{P \times M}$ and integers $V_1, V_2 \geq 0$, the notation $\mathbf{A}(s) \sim (V_1, V_2)$ indicates that there exist coefficient matrices $\mathbf{A}_v \in \mathbb{C}^{P \times M}, v = -V_1, -V_1 + 1, \dots, V_2$, such that

$$\mathbf{A}(s) = \sum_{v=-V_1}^{V_2} \mathbf{A}_v s^{-v}, \quad s \in \mathcal{U}. \quad (5)$$

If $\mathbf{A}(s) \sim (V_1, V_2)$, then $\mathbf{A}(s)$ is a *Laurent polynomial* (LP) matrix with *maximum degree* $V_1 + V_2$.

Before discussing interpolation, we briefly list the following statements which follow directly from Definition 3. First, $\mathbf{A}(s) \sim (V_1, V_2)$ implies $\mathbf{A}(s) \sim (V'_1, V'_2)$ for any $V'_1 \geq V_1, V'_2 \geq V_2$. Moreover, since for $s \in \mathcal{U}$ we have $s^* = s^{-1}$, $\mathbf{A}(s) \sim (V_1, V_2)$ implies $\mathbf{A}^H(s) \sim (V_2, V_1)$. Finally, given LP matrices $\mathbf{A}_1(s) \sim (V_{11}, V_{12})$ and $\mathbf{A}_2(s) \sim (V_{21}, V_{22})$, if $\mathbf{A}_1(s)$ and $\mathbf{A}_2(s)$ have the same dimensions, then $(\mathbf{A}_1(s) + \mathbf{A}_2(s)) \sim (\max(V_{11}, V_{21}), \max(V_{12}, V_{22}))$, whereas if the dimensions of $\mathbf{A}_1(s)$ and $\mathbf{A}_2(s)$ are such that the matrix product $\mathbf{A}_1(s)\mathbf{A}_2(s)$ is defined, then $\mathbf{A}_1(s)\mathbf{A}_2(s) \sim (V_{11} + V_{21}, V_{12} + V_{22})$.

In the remainder of this section, we review basic results on interpolation by considering the LP $a(s) \sim (V_1, V_2)$ with maximum degree $V \triangleq V_1 + V_2$. The following results can be directly extended to the interpolation of LP matrices through entrywise application. Borrowing terminology from signal analysis, we call the value of $a(s)$ at a given point $s_0 \in \mathcal{U}$ the *sample* $a(s_0)$.

Definition 4. *Interpolation* of the LP $a(s) \sim (V_1, V_2)$ from the set $\mathcal{B} = \{b_0, b_1, \dots, b_{B-1}\} \subset \mathcal{U}$, containing B distinct *base points*, to the set $\mathcal{T} = \{t_0, t_1, \dots, t_{T-1}\} \subset \mathcal{U}$, containing T distinct *target points*, is the process of obtaining the samples $a(t_0), a(t_1), \dots, a(t_{T-1})$ from the samples $a(b_0), a(b_1), \dots, a(b_{B-1})$, with knowledge of V_1 and V_2 , but without explicit knowledge of the coefficients $a_{-V_1}, a_{-V_1+1}, \dots, a_{V_2}$ that determine $a(s)$ according to (5).

In the following, we assume that $B \geq V + 1$. By defining the vectors $\mathbf{a} \triangleq [a_{-V_1} \ a_{-V_1+1} \ \dots \ a_{V_2}]^T$, $\mathbf{a}_{\mathcal{B}} \triangleq [a(b_0) \ a(b_1) \ \dots \ a(b_{B-1})]^T$, and $\mathbf{a}_{\mathcal{T}} \triangleq [a(t_0) \ a(t_1) \ \dots \ a(t_{T-1})]^T$, we note that $\mathbf{a}_{\mathcal{B}} = \mathbf{B}\mathbf{a}$, with the $B \times (V + 1)$ *base point matrix*

$$\mathbf{B} \triangleq \begin{bmatrix} b_0^{V_1} & b_0^{V_1-1} & \dots & b_0^{-V_2} \\ b_1^{V_1} & b_1^{V_1-1} & \dots & b_1^{-V_2} \\ \vdots & \vdots & \ddots & \vdots \\ b_{B-1}^{V_1} & b_{B-1}^{V_1-1} & \dots & b_{B-1}^{-V_2} \end{bmatrix} \quad (6)$$

and $\mathbf{a}_{\mathcal{T}} = \mathbf{T}\mathbf{a}$, with the $T \times (V + 1)$ *target point matrix*

$$\mathbf{T} \triangleq \begin{bmatrix} t_0^{V_1} & t_0^{V_1-1} & \dots & t_0^{-V_2} \\ t_1^{V_1} & t_1^{V_1-1} & \dots & t_1^{-V_2} \\ \vdots & \vdots & \ddots & \vdots \\ t_{T-1}^{V_1} & t_{T-1}^{V_1-1} & \dots & t_{T-1}^{-V_2} \end{bmatrix}. \quad (7)$$

Now, \mathbf{B} can be written as $\mathbf{B} = \mathbf{D}_{\mathcal{B}}\mathbf{V}_{\mathcal{B}}$, where $\mathbf{D}_{\mathcal{B}} \triangleq \text{diag}(b_0^{V_1}, b_1^{V_1}, \dots, b_{B-1}^{V_1})$ and $\mathbf{V}_{\mathcal{B}}$ is the $B \times (V + 1)$ Vandermonde matrix

$$\mathbf{V}_{\mathcal{B}} \triangleq \begin{bmatrix} 1 & b_0^{-1} & \dots & b_0^{-(V_1+V_2)} \\ 1 & b_1^{-1} & \dots & b_1^{-(V_1+V_2)} \\ \vdots & \vdots & \ddots & \vdots \\ 1 & b_{B-1}^{-1} & \dots & b_{B-1}^{-(V_1+V_2)} \end{bmatrix}.$$

Since the base points b_0, b_1, \dots, b_{B-1} are distinct, $\mathbf{V}_{\mathcal{B}}$ has full rank [9]. Hence, $\text{rank}(\mathbf{V}_{\mathcal{B}}) = V + 1$, which, together with the fact that $\mathbf{D}_{\mathcal{B}}$ is nonsingular, implies that $\text{rank}(\mathbf{B}) = V + 1$. Therefore, the coefficient vector \mathbf{a} is uniquely determined by the B samples of $a(s)$ at the base points b_0, b_1, \dots, b_{B-1} according to $\mathbf{a} = \mathbf{B}^\dagger \mathbf{a}_{\mathcal{B}}$, and interpolation of $a(s)$ from \mathcal{B} to \mathcal{T} can be performed by computing

$$\mathbf{a}_{\mathcal{T}} = \mathbf{T}\mathbf{B}^\dagger \mathbf{a}_{\mathcal{B}}. \quad (8)$$

In the remainder of the paper, we call the $T \times B$ matrix $\mathbf{T}\mathbf{B}^\dagger$ the *interpolation matrix*.

We conclude this section by noting that in the special case $V_1 = V_2$, we have $\mathbf{B} = \mathbf{B}^*\mathbf{E}$ and $\mathbf{T} = \mathbf{T}^*\mathbf{E}$, where the $(V + 1) \times (V + 1)$ matrix \mathbf{E} is obtained by flipping \mathbf{I}_{V+1} upside down. Since the operation of taking the pseudoinverse commutes with entrywise conjugation, it follows that $\mathbf{B}^\dagger = \mathbf{E}(\mathbf{B}^\dagger)^*$ and, as a consequence of $\mathbf{E}^2 = \mathbf{I}_{V+1}$, we obtain $\mathbf{T}\mathbf{B}^\dagger = (\mathbf{T}\mathbf{B}^\dagger)^*$, i.e., the interpolation matrix is real-valued.

3. Problem Statement

3.1. MIMO-OFDM System Model

We consider a MIMO system [13] with M_T transmit and M_R receive antennas. Throughout the paper, we focus on the case $M_R \geq M_T$. The matrix-valued impulse response of the frequency-selective MIMO channel is given by the taps $\mathbf{H}_l \in \mathbb{C}^{M_R \times M_T}$ ($l = 0, 1, \dots, L$) with the corresponding matrix-valued transfer function

$$\mathbf{H}(e^{j2\pi\theta}) = \sum_{l=0}^L \mathbf{H}_l e^{-j2\pi l\theta}, \quad 0 \leq \theta < 1$$

which satisfies $\mathbf{H}(s) \sim (0, L)$. In a MIMO-OFDM system with N OFDM tones and a cyclic prefix of length $L_{\text{CP}} \geq L$ samples, the equivalent input-output relation for the n th tone is given by

$$\mathbf{d}_n = \mathbf{H}(s_n)\mathbf{c}_n + \mathbf{w}_n, \quad n = 0, 1, \dots, N - 1$$

with the transmit signal vector $\mathbf{c}_n \triangleq [c_{n,1} \ c_{n,2} \ \cdots \ c_{n,M_T}]^T$, the receive signal vector $\mathbf{d}_n \triangleq [d_{n,1} \ d_{n,2} \ \cdots \ d_{n,M_R}]^T$, the additive noise vector \mathbf{w}_n , and $s_n \triangleq e^{j2\pi n/N}$. Here, $c_{n,m}$ stands for the complex-valued data symbol, taken from a finite constellation \mathcal{O} , transmitted by the m th antenna on the n th tone and $d_{n,m}$ is the signal observed at the m th receive antenna on the n th tone. For $n = 0, 1, \dots, N-1$, we assume that \mathbf{c}_n contains statistically independent entries and satisfies $\mathbb{E}[\mathbf{c}_n] = \mathbf{0}$ and $\mathbb{E}[\mathbf{c}_n^H \mathbf{c}_n] = 1$. Again for $n = 0, 1, \dots, N-1$, we assume that \mathbf{w}_n is statistically independent of \mathbf{c}_n and contains entries that are independent and identically distributed (i.i.d.) as $\mathcal{CN}(0, \sigma_w^2)$, where σ_w^2 denotes the noise variance and is assumed to be known at the receiver.

In practice, N is typically chosen to be a power of two in order to allow for efficient OFDM processing based on the Fast Fourier Transform (FFT). Moreover, a small subset of the N tones is typically set aside for pilot symbols and virtual tones at the frequency band edges, which help to reduce out-of-band interference and relax the pulse-shaping filter requirements. We collect the indices corresponding to the D tones carrying payload data into the set $\mathcal{D} \subseteq \{0, 1, \dots, N-1\}$. Typical OFDM systems have $D \geq 3L_{CP}$.

3.2. QR Decomposition in MIMO-OFDM Detectors

Widely used algorithms for coherent detection in MIMO-OFDM systems include successive cancellation (SC) detectors [13], both zero-forcing (ZF) and MMSE [21, 8], and sphere decoders, both in the original formulation [5, 17] requiring ZF-based preprocessing, as well as in the MMSE-based form proposed in [16]. These detection algorithms require QR decomposition in the preprocessing step, or, more specifically, computation of matrices $\mathbf{Q}(s_n)$ and $\mathbf{R}(s_n)$, for all $n \in \mathcal{D}$, defined as follows. In the ZF case, $\mathbf{Q}(s_n)$ and $\mathbf{R}(s_n)$ are QR factors of $\mathbf{H}(s_n)$, whereas in the MMSE case, $\mathbf{Q}(s_n)$ and $\mathbf{R}(s_n)$ are obtained as follows: $\bar{\mathbf{Q}}(s_n)\mathbf{R}(s_n)$ is the unique QR decomposition of the full-rank, $(M_R + M_T) \times M_T$ MMSE-augmented channel matrix

$$\bar{\mathbf{H}}(s_n) \triangleq \begin{bmatrix} \mathbf{H}(s_n) \\ \sqrt{M_T}\sigma_w \mathbf{I}_{M_T} \end{bmatrix} \quad (9)$$

and $\mathbf{Q}(s_n)$ is given by $\bar{\mathbf{Q}}^{1:M_R}(s_n)$. Taking the first M_R rows on both sides of the equation $\bar{\mathbf{H}}(s_n) = \bar{\mathbf{Q}}(s_n)\mathbf{R}(s_n)$ yields the factorization $\mathbf{H}(s_n) = \mathbf{Q}(s_n)\mathbf{R}(s_n)$, which is unique because of the uniqueness of $\bar{\mathbf{Q}}(s_n)$ and $\mathbf{R}(s_n)$, and which we call the *MMSE-QR decomposition* of $\mathbf{H}(s_n)$ with the *MMSE-QR factors* $\mathbf{Q}(s_n)$ and $\mathbf{R}(s_n)$.

In the following, we briefly describe how $\mathbf{Q}(s_n)$ and $\mathbf{R}(s_n)$, either derived as QR decomposition or as MMSE-QR decomposition of $\mathbf{H}(s_n)$, are used in the detection algorithms listed above. SC detectors essentially solve the linear system of equations $\mathbf{Q}^H(s_n)\mathbf{d}_n = \mathbf{R}(s_n)\hat{\mathbf{c}}_n$ by back-substitution (with rounding of the intermediate results to elements of \mathcal{O} [13]) to obtain $\hat{\mathbf{c}}_n \in \mathcal{O}^{M_T}$. Sphere decoders exploit the upper triangularity of $\mathbf{R}(s_n)$ to find the symbol vector $\hat{\mathbf{c}}_n \in \mathcal{O}^{M_T}$ that minimizes $\|\mathbf{Q}^H(s_n)\mathbf{d}_n - \mathbf{R}(s_n)\hat{\mathbf{c}}_n\|^2$ through an efficient tree search [17].

3.3. Problem Statement

We assume that the MIMO-OFDM receiver has perfect knowledge of the samples $\mathbf{H}(s_n)$ for $n \in \mathcal{E} \subseteq \{0, 1, \dots, N-1\}$, with $|\mathcal{E}| \geq L+1$, from which $\mathbf{H}(s_n)$ can be obtained at any data-carrying tone $n \in \mathcal{D}$ through interpolation of $\mathbf{H}(s) \sim (0, L)$. We note that interpolation of $\mathbf{H}(s)$ is not necessary if $\mathcal{D} \subseteq \mathcal{E}$. We next formulate the problem statement by focusing on ZF-based detectors, which require QR decomposition of the MIMO-OFDM channel matrices $\mathbf{H}(s_n)$. The problem statement for the MMSE case is analogous with QR decomposition replaced by MMSE-QR decomposition.

The MIMO-OFDM receiver needs to compute QR factors $\mathbf{Q}(s_n)$ and $\mathbf{R}(s_n)$ of $\mathbf{H}(s_n)$ for all data-carrying tones $n \in \mathcal{D}$. A straightforward approach to solving this problem consists of first interpolating $\mathbf{H}(s)$ to obtain $\mathbf{H}(s_n)$ at the tones $n \in \mathcal{D}$ and then performing QR decomposition on a per-tone basis. This method will henceforth be called *brute-force per-tone QR decomposition*. The interpolation-based QR decomposition algorithms presented in this paper are motivated by the following observations. First, performing QR decomposition on an $M \times M$ matrix requires $O(M^3)$ arithmetic operations [6], whereas the number of arithmetic operations involved in computing one sample of an $M \times M$ LP matrix by interpolation is proportional to the number of matrix entries M^2 , as interpolation of an LP matrix is performed entrywise. This comparison suggests that we may obtain fundamental savings in computational complexity by replacing QR decomposition by interpolation. Second, consider a flat-fading channel, so that $L = 0$ and hence $\mathbf{H}(s_n) = \mathbf{H}_0$ for all $n = 0, 1, \dots, N-1$. In this case, a single QR decomposition $\mathbf{H}_0 = \mathbf{QR}$ yields QR factors of $\mathbf{H}(s_n)$ for all data-carrying tones $n \in \mathcal{D}$. A question that now arises naturally is whether for $L > 0$ QR factors $\mathbf{Q}(s_n)$ and $\mathbf{R}(s_n)$, $n \in \mathcal{D}$, can be obtained from a smaller set of QR factors through interpolation. We will see that the answer is in the affirmative and will, moreover, demonstrate that interpolation-based QR decomposition algorithms can yield significant computational complexity savings over brute-force per-tone QR decomposition for a wide range of values of the parameters M_T , M_R , L , N , and D , which will be referred to as *the system parameters* throughout the paper. The key to formulating interpolation-based algorithms and realizing these complexity savings is a result on QR decomposition of LP matrices formalized in Theorem 9 in the next section.

4. QR Decomposition through Interpolation

4.1. Additional Properties of QR Decomposition

We next set the stage for the formulation of our main technical result by presenting additional properties of QR decomposition of a matrix $\mathbf{A} \in \mathbb{C}^{P \times M}$, with $P \geq M$, that are directly implied by Definition 1.

Proposition 5. *Let $\mathbf{A} = \mathbf{QR}$ be a QR decomposition of \mathbf{A} . Then, for a given $k \in \{1, 2, \dots, M\}$, $\mathbf{A}_{1,k} = \mathbf{Q}_{1,k} \mathbf{R}_{1,k}^{1,k}$ is a QR decomposition of $\mathbf{A}_{1,k}$.*

Proof. From $\mathbf{A} = \mathbf{QR}$ it follows that $\mathbf{A}_{1,k} = (\mathbf{QR})_{1,k} = \mathbf{Q}_{1,k}\mathbf{R}_{1,k}^{1,k} + \mathbf{Q}_{k+1,M}\mathbf{R}_{1,k}^{k+1,M}$, which simplifies to $\mathbf{A}_{1,k} = \mathbf{Q}_{1,k}\mathbf{R}_{1,k}^{1,k}$, since the upper triangularity of \mathbf{R} implies $\mathbf{R}_{1,k}^{k+1,M} = \mathbf{0}$. $\mathbf{Q}_{1,k}$ and $\mathbf{R}_{1,k}^{1,k}$ satisfy Conditions 1 and 2 of Definition 1 since all columns of $\mathbf{Q}_{1,k}$ are also columns of \mathbf{Q} and since $\mathbf{R}_{1,k}^{1,k}$ is a principal submatrix of \mathbf{R} , respectively. Finally, $\mathbf{R} = \mathbf{Q}^H\mathbf{A}$ implies $\mathbf{R}_{1,k}^{1,k} = (\mathbf{Q}^H\mathbf{A})_{1,k}^{1,k} = \mathbf{Q}_{1,k}^H\mathbf{A}_{1,k}$ and hence Condition 3 of Definition 1 is satisfied. \square

Proposition 6. *Let $\mathbf{A} = \mathbf{QR}$ be a QR decomposition of \mathbf{A} . Then, for $M > 1$ and for a given $k \in \{2, 3, \dots, M\}$, $\mathbf{A}_{k,M} - \mathbf{Q}_{1,k-1}\mathbf{R}_{k,M}^{1,k-1} = \mathbf{Q}_{k,M}\mathbf{R}_{k,M}^{k,M}$ is a QR decomposition of $\mathbf{A}_{k,M} - \mathbf{Q}_{1,k-1}\mathbf{R}_{k,M}^{1,k-1}$.*

Proof. $\mathbf{A} = \mathbf{Q}_{1,k-1}\mathbf{R}^{1,k-1} + \mathbf{Q}_{k,M}\mathbf{R}^{k,M}$ implies $\mathbf{A}_{k,M} = \mathbf{Q}_{1,k-1}\mathbf{R}_{k,M}^{1,k-1} + \mathbf{Q}_{k,M}\mathbf{R}_{k,M}^{k,M}$ and hence $\mathbf{A}_{k,M} - \mathbf{Q}_{1,k-1}\mathbf{R}_{k,M}^{1,k-1} = \mathbf{Q}_{k,M}\mathbf{R}_{k,M}^{k,M}$. $\mathbf{Q}_{k,M}$ and $\mathbf{R}_{k,M}^{k,M}$ satisfy Conditions 1 and 2 of Definition 1 since all columns of $\mathbf{Q}_{k,M}$ are also columns of \mathbf{Q} and since $\mathbf{R}_{k,M}^{k,M}$ is a principal submatrix of \mathbf{R} , respectively. Moreover, $\mathbf{R} = \mathbf{Q}^H\mathbf{A}$ implies $\mathbf{R}_{k,M}^{k,M} = (\mathbf{Q}^H\mathbf{A})_{k,M}^{k,M} = \mathbf{Q}_{k,M}^H\mathbf{A}_{k,M}$. Using $\mathbf{Q}_{k,M}^H\mathbf{Q}_{1,k-1} = \mathbf{0}$, which follows from the fact that the nonzero columns of \mathbf{Q} are orthonormal, we can write $\mathbf{R}_{k,M}^{k,M} = \mathbf{Q}_{k,M}^H\mathbf{A}_{k,M} - \mathbf{Q}_{k,M}^H\mathbf{Q}_{1,k-1}\mathbf{R}_{k,M}^{1,k-1} = \mathbf{Q}_{k,M}^H(\mathbf{A}_{k,M} - \mathbf{Q}_{1,k-1}\mathbf{R}_{k,M}^{1,k-1})$. Hence, Condition 3 of Definition 1 is satisfied. \square

In order to characterize QR decomposition of \mathbf{A} in the general case $\text{rank}(\mathbf{A}) \leq M$, we introduce the following concept.

Definition 7. The *ordered column rank* of \mathbf{A} is the number

$$K \triangleq \begin{cases} 0, & \text{rank}(\mathbf{A}_{1,1}) = 0 \\ \max\{k \in \{1, 2, \dots, M\} : \text{rank}(\mathbf{A}_{1,k}) = k\}, & \text{else.} \end{cases}$$

For later use, we note that $K = 0$ is equivalent to $\mathbf{a}_1 = \mathbf{0}$, and that $K < M$ is equivalent to \mathbf{A} being rank-deficient.

Proposition 8. *QR factors \mathbf{Q} and \mathbf{R} of a matrix \mathbf{A} of ordered column rank $K > 0$ satisfy the following properties:*

1. $\mathbf{Q}_{1,K}^H\mathbf{Q}_{1,K} = \mathbf{I}_K$
2. $[\mathbf{R}]_{k,k} > 0$ for $k = 1, 2, \dots, K$
3. $\mathbf{Q}_{1,K}$ and $\mathbf{R}^{1,K}$ are unique
4. $\text{ran}(\mathbf{Q}_{1,k}) = \text{ran}(\mathbf{A}_{1,k})$ for $k = 1, 2, \dots, K$
5. if $K < M$, $[\mathbf{R}]_{K+1,K+1} = 0$

Proof. Since $\mathbf{Q}_{1,K}$ and $\mathbf{R}_{1,K}^{1,K}$ are QR factors of $\mathbf{A}_{1,K}$, as stated in Proposition 5, and since $\text{rank}(\mathbf{A}_{1,K}) = K$, Properties 1 and 2, as well as the uniqueness of $\mathbf{Q}_{1,K}$ stated in Property 3, are obtained directly by applying Proposition 2 to the full-rank matrix $\mathbf{A}_{1,K}$. The uniqueness of $\mathbf{R}^{1,K}$ stated in Property 3 is implied by the uniqueness of $\mathbf{Q}_{1,K}$ and by $\mathbf{R}^{1,K} = \mathbf{Q}_{1,K}^H\mathbf{A}$, which follows from Condition 3 of Definition 1. For

$k = 1, 2, \dots, K$, $\text{ran}(\mathbf{Q}_{1,k}) = \text{ran}(\mathbf{A}_{1,k})$ is a trivial consequence of $\mathbf{A}_{1,k} = \mathbf{Q}_{1,k}\mathbf{R}_{1,k}^{1,k}$ and of $\text{rank}(\mathbf{R}_{1,k}^{1,k}) = k$, which follows from the fact that $\mathbf{R}_{1,k}^{1,k}$ is upper triangular with nonzero entries on its main diagonal. This proves Property 4. If $K < M$, Condition 3 of Definition 1 implies $[\mathbf{R}]_{K+1,K+1} = \mathbf{q}_{K+1}^H \mathbf{a}_{K+1}$. If $\mathbf{q}_{K+1} = \mathbf{0}$, $[\mathbf{R}]_{K+1,K+1} = 0$ follows trivially. If $\mathbf{q}_{K+1} \neq \mathbf{0}$, Condition 1 of Definition 1 implies that \mathbf{q}_{K+1} is orthogonal to $\text{ran}(\mathbf{Q}_{1,K})$, whereas the definition of K implies that $\mathbf{a}_{K+1} \in \text{ran}(\mathbf{A}_{1,K})$. Since $\text{ran}(\mathbf{Q}_{1,K}) = \text{ran}(\mathbf{A}_{1,K})$, we obtain $\mathbf{q}_{K+1}^H \mathbf{a}_{K+1} = [\mathbf{R}]_{K+1,K+1} = 0$, which proves Property 5. \square

We emphasize that for $K > 0$, the uniqueness of $\mathbf{Q}_{1,K}$ and $\mathbf{R}^{1,K}$ has two significant consequences. First, the GS orthonormalization procedure (1)–(3), evaluated for $k = 1, 2, \dots, K$, determines the submatrices $\mathbf{Q}_{1,K}$ and $\mathbf{R}^{1,K}$ of the matrices \mathbf{Q} and \mathbf{R} produced by *any* QR decomposition algorithm. Second, the nonuniqueness of \mathbf{Q} and \mathbf{R} in the case of rank-deficient \mathbf{A} , demonstrated in Section 2.2, is restricted to the submatrices $\mathbf{Q}_{K+1,M}$ and $\mathbf{R}^{K+1,M}$.

Finally, we note that Property 5 of Proposition 8 is valid for the case $K = 0$ as well. In fact, Condition 3 of Definition 1 implies $[\mathbf{R}]_{1,1} = \mathbf{q}_1^H \mathbf{a}_1$. Since $K = 0$ implies $\mathbf{a}_1 = \mathbf{0}$, we immediately obtain $[\mathbf{R}]_{1,1} = 0$.

4.2. QR Decomposition of an LP Matrix

In the remainder of Section 4, we consider a $P \times M$ LP matrix $\mathbf{A}(s) \sim (V_1, V_2)$, $s \in \mathcal{U}$, with $P \geq M$, and QR factors $\mathbf{Q}(s)$ and $\mathbf{R}(s)$ of $\mathbf{A}(s)$. Despite $\mathbf{A}(s)$ being an LP matrix, $\mathbf{Q}(s)$ and $\mathbf{R}(s)$ will, in general, not be LP matrices. To see this, consider the case where $\text{rank}(\mathbf{A}(s)) = M$ for all $s \in \mathcal{U}$. It follows from the results in Sections 2.2 and 4.1 that, in this case, $\mathbf{Q}(s)$ and $\mathbf{R}(s)$ are unique and determined through (1)–(3). The division and the square root operation in (2), in general, prevent $\mathbf{Q}(s)$, and hence also $\mathbf{R}(s) = \mathbf{Q}^H(s)\mathbf{A}(s)$, from being LP matrices. Nevertheless, in this section we will show that there exists a mapping \mathcal{M} that transforms $\mathbf{Q}(s)$ and $\mathbf{R}(s)$ into corresponding LP matrices $\tilde{\mathbf{Q}}(s)$ and $\tilde{\mathbf{R}}(s)$. The mapping \mathcal{M} constitutes the basis for the formulation of interpolation-based QR decomposition algorithms for MIMO-OFDM systems.

In the following, we consider QR factors of $\mathbf{A}(s_0)$ for a given $s_0 \in \mathcal{U}$. In order to keep the notation compact, we omit the dependence of all involved quantities on s_0 . We start by defining the auxiliary variables Δ_k as

$$\Delta_k \triangleq \Delta_{k-1} [\mathbf{R}]_{k,k}^2, \quad k = 1, 2, \dots, M \quad (10)$$

with $\Delta_0 \triangleq 1$. Next, we introduce the vectors

$$\tilde{\mathbf{q}}_k \triangleq \Delta_{k-1} [\mathbf{R}]_{k,k} \mathbf{q}_k, \quad k = 1, 2, \dots, M \quad (11)$$

$$\tilde{\mathbf{r}}_k^T \triangleq \Delta_{k-1} [\mathbf{R}]_{k,k} \mathbf{r}_k^T, \quad k = 1, 2, \dots, M \quad (12)$$

and define the mapping $\mathcal{M} : (\mathbf{Q}, \mathbf{R}) \mapsto (\tilde{\mathbf{Q}}, \tilde{\mathbf{R}})$ by $\tilde{\mathbf{Q}} \triangleq [\tilde{\mathbf{q}}_1 \ \tilde{\mathbf{q}}_2 \ \dots \ \tilde{\mathbf{q}}_M]$ and $\tilde{\mathbf{R}} \triangleq [\tilde{\mathbf{r}}_1 \ \tilde{\mathbf{r}}_2 \ \dots \ \tilde{\mathbf{r}}_M]^T$.

Now, we consider the ordered column rank K of \mathbf{A} , and note that Property 2 in Proposition 8 implies that, if $K > 0$, $\Delta_{k-1} [\mathbf{R}]_{k,k} > 0$ for $k = 1, 2, \dots, K$, as seen by unfolding the recursion in (10). Hence, for

$K > 0$ and $k = 1, 2, \dots, K$, we can compute \mathbf{q}_k and \mathbf{r}_k^T from $\tilde{\mathbf{q}}_k$ and $\tilde{\mathbf{r}}_k^T$, respectively, according to

$$\mathbf{q}_k = (\Delta_{k-1} [\mathbf{R}]_{k,k})^{-1} \tilde{\mathbf{q}}_k \quad (13)$$

$$\mathbf{r}_k^T = (\Delta_{k-1} [\mathbf{R}]_{k,k})^{-1} \tilde{\mathbf{r}}_k^T \quad (14)$$

where $\Delta_{k-1} [\mathbf{R}]_{k,k}$ is obtained from the entries on the main diagonal of $\tilde{\mathbf{R}}$ as

$$\Delta_{k-1} [\mathbf{R}]_{k,k} = \begin{cases} \sqrt{[\tilde{\mathbf{R}}]_{k,k}}, & k = 1 \\ \sqrt{[\tilde{\mathbf{R}}]_{k-1,k-1} [\tilde{\mathbf{R}}]_{k,k}}, & k = 2, 3, \dots, K. \end{cases} \quad (15)$$

If $K = M$, i.e., for full-rank \mathbf{A} , we have $\Delta_{k-1} [\mathbf{R}]_{k,k} \neq 0$ for all $k = 1, 2, \dots, M$, and the mapping \mathcal{M} is invertible. In the case $K < M$, Property 5 in Proposition 8 states that $[\mathbf{R}]_{K+1,K+1} = \mathbf{0}$, which combined with (10)–(12) implies that $\Delta_k = 0$, $\tilde{\mathbf{q}}_k = \mathbf{0}$, and $\tilde{\mathbf{r}}_k^T = \mathbf{0}$ for $k = K+1, K+2, \dots, M$. Hence, the mapping \mathcal{M} is not invertible for $K < M$, since the information contained in $\mathbf{Q}_{K+1,M}$ and $\mathbf{R}^{K+1,M}$ can not be extracted from $\tilde{\mathbf{Q}}_{K+1,M} = \mathbf{0}$ and $\tilde{\mathbf{R}}^{K+1,M} = \mathbf{0}$. Nevertheless, we can recover $\mathbf{Q}_{K+1,M}$ and $\mathbf{R}^{K+1,M}$ as follows. For $0 < K < M$, setting $k = K+1$ in Proposition 6 shows that $\mathbf{Q}_{K+1,M}$ and $\mathbf{R}_{K+1,M}^{K+1,M}$ can be obtained by QR decomposition of $\mathbf{A}_{K+1,M} - \mathbf{Q}_{1,K} \mathbf{R}_{K+1,M}^{1,K}$. Then, $\mathbf{R}^{K+1,M}$ is obtained as $\mathbf{R}^{K+1,M} = [\mathbf{R}_{1,K}^{K+1,M} \quad \mathbf{R}_{K+1,M}^{K+1,M}]$ with $\mathbf{R}_{1,K}^{K+1,M} = \mathbf{0}$ because of the upper triangularity of \mathbf{R} . For $K = 0$, since $\tilde{\mathbf{Q}}$ and $\tilde{\mathbf{R}}$ are all-zero matrices, $\mathbf{Q}_{K+1,M} = \mathbf{Q}$ and $\mathbf{R}_{K+1,M}^{K+1,M} = \mathbf{R}$ must be obtained by performing QR decomposition on \mathbf{A} . In the remainder of the paper, we denote by *inverse mapping* $\mathcal{M}^{-1} : (\tilde{\mathbf{Q}}, \tilde{\mathbf{R}}) \mapsto (\mathbf{Q}, \mathbf{R})$ the procedure¹ formulated in the following steps:

1. If $K > 0$, for $k = 1, 2, \dots, K$, compute the scaling factor $(\Delta_{k-1} [\mathbf{R}]_{k,k})^{-1}$ using (15) and scale $\tilde{\mathbf{q}}_k$ and $\tilde{\mathbf{r}}_k^T$ according to (13) and (14), respectively.
2. If $0 < K < M$, compute $\mathbf{Q}_{K+1,M}$ and $\mathbf{R}_{K+1,M}^{K+1,M}$ by performing QR decomposition on $\mathbf{A}_{K+1,M} - \mathbf{Q}_{1,K} \mathbf{R}_{K+1,M}^{1,K}$, and construct $\mathbf{R}^{K+1,M} = [\mathbf{0} \quad \mathbf{R}_{K+1,M}^{K+1,M}]$.
3. If $K = 0$, compute \mathbf{Q} and \mathbf{R} by performing QR decomposition on \mathbf{A} .

We note that the nonuniqueness of QR decomposition in the case $K < M$ has the following consequence. Given QR factors \mathbf{Q}_1 and \mathbf{R}_1 of \mathbf{A} , the application of the mapping \mathcal{M} to $(\mathbf{Q}_1, \mathbf{R}_1)$ followed by application of the inverse mapping \mathcal{M}^{-1} yields matrices \mathbf{Q}_2 and \mathbf{R}_2 that may not be equal to \mathbf{Q}_1 and \mathbf{R}_1 , respectively. However, \mathbf{Q}_2 and \mathbf{R}_2 are QR factors of \mathbf{A} in the sense of Definition 1.

We are now ready to present the main technical result of this paper. This result paves the way for the formulation of interpolation-based QR decomposition algorithms.

Theorem 9. *Given $\mathbf{A} : \mathcal{U} \rightarrow \mathbb{C}^{P \times M}$ with $P \geq M$, such that $\mathbf{A}(s) \sim (V_1, V_2)$ with maximum degree $V = V_1 + V_2$. The functions $\Delta_k(s)$, $\tilde{\mathbf{q}}_k(s)$, and $\tilde{\mathbf{r}}_k^T(s)$, obtained by applying the mapping \mathcal{M} as in (10)–(12) to QR factors $\mathbf{Q}(s)$ and $\mathbf{R}(s)$ of $\mathbf{A}(s)$ for all $s \in \mathcal{U}$, satisfy the following properties:*

¹Note that for $K < M$, the inverse mapping \mathcal{M}^{-1} requires explicit knowledge of $\mathbf{A}_{K+1,M}$.

1. $\Delta_k(s) \sim (kV, kV)$
2. $\tilde{\mathbf{q}}_k(s) \sim ((k-1)V + V_1, (k-1)V + V_2)$
3. $\tilde{\mathbf{r}}_k^T(s) \sim (kV, kV)$.

We emphasize that Theorem 9 applies to any QR factors satisfying Definition 1 and is therefore not affected by the nonuniqueness of QR decomposition arising in the rank-deficient case.

Before proceeding to the proof, we note that Theorem 9 implies that the maximum degrees of the LP matrices $\tilde{\mathbf{Q}}(s)$ and $\tilde{\mathbf{R}}(s)$ are $(2M-1)V$ and $2MV$, respectively. We can therefore conclude that $2MV+1$ base points are enough for interpolation of both $\tilde{\mathbf{Q}}(s)$ and $\tilde{\mathbf{R}}(s)$. We mention that the results presented in [4], in the context of narrowband MIMO systems, involving a QR decomposition algorithm that avoids divisions and square root operations, can be applied to the problem at hand as well. This leads to an alternative mapping of $\mathbf{Q}(s)$ and $\mathbf{R}(s)$ to LP matrices with maximum degrees significantly higher than $2MV$.

4.3. Proof of Theorem 9

The proof consists of three steps, summarized as follows. In Step 1, we focus on a given $s_0 \in \mathcal{U}$ and aim at writing $\Delta_k(s_0)$, $\tilde{\mathbf{q}}_k(s_0)$, and $\tilde{\mathbf{r}}_k^T(s_0)$ as functions of $\mathbf{A}(s_0)$ for all $(K(s_0), k) \in \mathcal{K} \triangleq \{0, 1, \dots, M\} \times \{1, 2, \dots, M\}$, where $K(s_0)$ denotes the ordered column rank of $\mathbf{A}(s_0)$. Step 1 is split into Steps 1a and 1b, in which the two disjoint subsets $\mathcal{K}_1 \triangleq \{(K', k') \in \mathcal{K} : 0 < K' \leq M, 1 \leq k' \leq K'\}$ and $\mathcal{K}_2 \triangleq \{(K', k') \in \mathcal{K} : 0 \leq K' < M, K' + 1 \leq k' \leq M\}$ (with $\mathcal{K}_1 \cup \mathcal{K}_2 = \mathcal{K}$) are considered, respectively. In Step 1a, we note that for $(K(s_0), k) \in \mathcal{K}_1$, $\mathbf{Q}_{1, K(s_0)}(s_0)$ and $\mathbf{R}^{1, K(s_0)}(s_0)$ are unique and can be obtained by evaluating (1)–(3) for $k = 1, 2, \dots, K(s_0)$. By unfolding the recursions in (1)–(3) and in (10)–(12), we write $\Delta_k(s_0)$, $\tilde{\mathbf{q}}_k(s_0)$, and $\tilde{\mathbf{r}}_k^T(s_0)$ as functions of $\mathbf{A}(s_0)$ for $(K(s_0), k) \in \mathcal{K}_1$. In Step 1b, we show that the expressions for $\Delta_k(s_0)$, $\tilde{\mathbf{q}}_k(s_0)$, and $\tilde{\mathbf{r}}_k^T(s_0)$, derived in Step 1a for $(K(s_0), k) \in \mathcal{K}_1$, are also valid for $(K(s_0), k) \in \mathcal{K}_2$ and hence, as a consequence of $\mathcal{K}_1 \cup \mathcal{K}_2 = \mathcal{K}$, for all $(K(s_0), k) \in \mathcal{K}$. In Step 2, we note that the derivations in Step 1 carry over to all $s_0 \in \mathcal{U}$, and generalize the expressions obtained in Step 1 to expressions for $\Delta_k(s)$, $\tilde{\mathbf{q}}_k(s)$, and $\tilde{\mathbf{r}}_k^T(s)$ that hold for $k = 1, 2, \dots, M$ and for all $s \in \mathcal{U}$. Making use of $\mathbf{A}(s) \sim (V_1, V_2)$, in Step 3 it is finally shown that $\Delta_k(s)$, $\tilde{\mathbf{q}}_k(s)$, and $\tilde{\mathbf{r}}_k^T(s)$ satisfy Properties 1–3 in the statement of Theorem 9.

Step 1a. Throughout Steps 1a and 1b, in order to simplify the notation, we drop the dependence of all quantities on s_0 . In Step 1a, we assume that $(K, k) \in \mathcal{K}_1$ and, unless stated otherwise, all equations and statements involving k are valid for all $k = 1, 2, \dots, K$.

We start by listing preparatory results. We recall from Section 4.1 that the submatrices $\mathbf{Q}_{1, K}$ and $\mathbf{R}^{1, K}$ are unique and that, consequently, \mathbf{q}_k and \mathbf{r}_k^T are determined by (1)–(3). From $\mathbf{q}_k \neq \mathbf{0}$, implied by Property 1 in Proposition 8, and from (2) we deduce that $\mathbf{y}_k \neq \mathbf{0}$. Then, from (1) and (2) we obtain

$$\mathbf{y}_k^H \mathbf{y}_k = \mathbf{y}_k^H \mathbf{a}_k - \sum_{i=1}^{k-1} \mathbf{q}_i^H \mathbf{a}_k \sqrt{\mathbf{y}_k^H \mathbf{y}_k \mathbf{q}_i^H \mathbf{q}_i} = \mathbf{y}_k^H \mathbf{a}_k \quad (16)$$

as $\mathbf{q}_k^H \mathbf{q}_i = 0$ for $i = 1, 2, \dots, k-1$. Consequently, we can write $[\mathbf{R}]_{k,k}$, using (2) and (3), as

$$[\mathbf{R}]_{k,k} = \mathbf{q}_k^H \mathbf{a}_k = \frac{\mathbf{y}_k^H \mathbf{a}_k}{\sqrt{\mathbf{y}_k^H \mathbf{y}_k}} = \sqrt{\mathbf{y}_k^H \mathbf{y}_k} \quad (17)$$

thus implying $[\mathbf{R}]_{k,k} \mathbf{q}_k = \mathbf{y}_k$ and hence, by (11),

$$\tilde{\mathbf{q}}_k = \Delta_{k-1} \mathbf{y}_k. \quad (18)$$

Furthermore, using (10) and (17), we can write $\Delta_k = \Delta_{k-1} \mathbf{y}_k^H \mathbf{y}_k$ or alternatively, in recursion-free form,

$$\Delta_k = \prod_{i=1}^k \mathbf{y}_i^H \mathbf{y}_i. \quad (19)$$

Next, we note that (1) implies

$$\mathbf{y}_k = \mathbf{a}_k + \sum_{i=1}^{k-1} \alpha_i^{(k)} \mathbf{a}_i \quad (20)$$

with unique coefficients $\alpha_i^{(k)}$, $i = 1, 2, \dots, k-1$, since $\mathbf{y}_1 = \mathbf{a}_1$ and since for $k > 1$, we have $\text{rank}(\mathbf{A}_{1,k-1}) = k-1$ and, as stated in Property 4 of Proposition 8, $\text{ran}(\mathbf{Q}_{1,k-1}) = \text{ran}(\mathbf{A}_{1,k-1})$. Next, we consider the relation between $\{\mathbf{a}_1, \mathbf{a}_2, \dots, \mathbf{a}_k\}$ and $\{\mathbf{y}_1, \mathbf{y}_2, \dots, \mathbf{y}_k\}$. Inserting (2) into (1) yields

$$\mathbf{y}_k = \mathbf{a}_k - \sum_{i=1}^{k-1} \frac{\mathbf{y}_i^H \mathbf{a}_k}{\mathbf{y}_i^H \mathbf{y}_i} \mathbf{y}_i.$$

Hence, using (16), we obtain

$$\begin{aligned} \mathbf{a}_{k'} &= \mathbf{y}_{k'} + \sum_{i=1}^{k'-1} \frac{\mathbf{y}_i^H \mathbf{a}_{k'}}{\mathbf{y}_i^H \mathbf{y}_i} \mathbf{y}_i \\ &= \sum_{i=1}^{k'} \frac{\mathbf{y}_i^H \mathbf{a}_{k'}}{\mathbf{y}_i^H \mathbf{y}_i} \mathbf{y}_i, \quad k' = 1, 2, \dots, k. \end{aligned} \quad (21)$$

We next note that (21) can be rewritten, for $k' = 1, 2, \dots, k$, in vector-matrix form as

$$[\mathbf{a}_1 \ \mathbf{a}_2 \ \cdots \ \mathbf{a}_k] = [\mathbf{y}_1 \ \mathbf{y}_2 \ \cdots \ \mathbf{y}_k] \mathbf{V}_k \quad (22)$$

with the $k \times k$ matrix

$$\mathbf{V}_k \triangleq \begin{bmatrix} \frac{\mathbf{y}_1^H \mathbf{a}_1}{\mathbf{y}_1^H \mathbf{y}_1} & \frac{\mathbf{y}_1^H \mathbf{a}_2}{\mathbf{y}_1^H \mathbf{y}_1} & \cdots & \frac{\mathbf{y}_1^H \mathbf{a}_k}{\mathbf{y}_1^H \mathbf{y}_1} \\ 0 & \frac{\mathbf{y}_2^H \mathbf{a}_2}{\mathbf{y}_2^H \mathbf{y}_2} & \cdots & \frac{\mathbf{y}_2^H \mathbf{a}_k}{\mathbf{y}_2^H \mathbf{y}_2} \\ \vdots & \vdots & \ddots & \vdots \\ 0 & 0 & \cdots & \frac{\mathbf{y}_k^H \mathbf{a}_k}{\mathbf{y}_k^H \mathbf{y}_k} \end{bmatrix}$$

satisfying $\det(\mathbf{V}_k) = 1$ because of $\mathbf{y}_k \neq \mathbf{0}$ and of (16). Next, we can write \mathbf{V}_k as $\mathbf{V}_k = \mathbf{D}_k^{-1} \mathbf{U}_k$ with the $k \times k$ nonsingular matrices $\mathbf{D}_k \triangleq \text{diag}(\mathbf{y}_1^H \mathbf{y}_1, \mathbf{y}_2^H \mathbf{y}_2, \dots, \mathbf{y}_k^H \mathbf{y}_k)$ and

$$\mathbf{U}_k \triangleq \begin{bmatrix} \mathbf{y}_1^H \mathbf{a}_1 & \mathbf{y}_1^H \mathbf{a}_2 & \cdots & \mathbf{y}_1^H \mathbf{a}_k \\ 0 & \mathbf{y}_2^H \mathbf{a}_2 & \cdots & \mathbf{y}_2^H \mathbf{a}_k \\ \vdots & \vdots & \ddots & \vdots \\ 0 & 0 & \cdots & \mathbf{y}_k^H \mathbf{a}_k \end{bmatrix}. \quad (23)$$

We next express Δ_k as a function of $\mathbf{A}_{1,k}$. From (16), (19), and (23), we obtain

$$\Delta_k = \prod_{i=1}^k \mathbf{y}_i^H \mathbf{a}_i = \det(\mathbf{U}_k). \quad (24)$$

Furthermore, (2), (3), and (17) imply

$$\mathbf{y}_{k'}^H \mathbf{a}_i = \sqrt{\mathbf{y}_{k'}^H \mathbf{y}_{k'}} \mathbf{q}_{k'}^H \mathbf{a}_i = [\mathbf{R}]_{k',k'} [\mathbf{R}]_{k',i}$$

which evaluates to zero for $1 \leq i < k' \leq k$ because of the upper triangularity of \mathbf{R} . Hence, \mathbf{U}_k can be written as

$$\mathbf{U}_k = \begin{bmatrix} \mathbf{y}_1^H \mathbf{a}_1 & \mathbf{y}_1^H \mathbf{a}_2 & \cdots & \mathbf{y}_1^H \mathbf{a}_k \\ \mathbf{y}_2^H \mathbf{a}_1 & \mathbf{y}_2^H \mathbf{a}_2 & \cdots & \mathbf{y}_2^H \mathbf{a}_k \\ \vdots & \vdots & \ddots & \vdots \\ \mathbf{y}_{k'}^H \mathbf{a}_1 & \mathbf{y}_{k'}^H \mathbf{a}_2 & \cdots & \mathbf{y}_{k'}^H \mathbf{a}_k \\ \vdots & \vdots & \ddots & \vdots \\ \mathbf{y}_k^H \mathbf{a}_1 & \mathbf{y}_k^H \mathbf{a}_2 & \cdots & \mathbf{y}_k^H \mathbf{a}_k \end{bmatrix}. \quad (25)$$

By combining (24) and (25), we obtain

$$\Delta_k = \det(\mathbf{U}_k) = \det \begin{bmatrix} \mathbf{y}_1^H \mathbf{A}_{1,k} \\ \mathbf{y}_2^H \mathbf{A}_{1,k} \\ \vdots \\ \mathbf{y}_{k'}^H \mathbf{A}_{1,k} \end{bmatrix} = \det \begin{bmatrix} \mathbf{a}_1^H \mathbf{A}_{1,k} \\ \mathbf{a}_2^H \mathbf{A}_{1,k} \\ \vdots \\ \mathbf{a}_{k'}^H \mathbf{A}_{1,k} \end{bmatrix} \quad (26)$$

$$= \det(\mathbf{A}_{1,k}^H \mathbf{A}_{1,k}) \quad (27)$$

where the third equality in (26) can be shown by induction as follows. We start by noting that $\mathbf{y}_1 = \mathbf{a}_1$, which implies that in the first row of \mathbf{U}_k , \mathbf{y}_1 can be replaced by \mathbf{a}_1 . For $k' > 1$, assuming that we have already replaced $\mathbf{y}_1, \mathbf{y}_2, \dots, \mathbf{y}_{k'-1}$ by $\mathbf{a}_1, \mathbf{a}_2, \dots, \mathbf{a}_{k'-1}$, respectively, we can replace $\mathbf{y}_{k'}$ by $\mathbf{a}_{k'}$ since, as a consequence of (20), the k' th row of \mathbf{U}_k can be written as

$$\mathbf{y}_{k'}^H \mathbf{A}_{1,k} = \mathbf{a}_{k'}^H \mathbf{A}_{1,k} + \sum_{i=1}^{k'-1} (\alpha_i^{(k')})^* (\mathbf{a}_i^H \mathbf{A}_{1,k}).$$

Hence, replacing $\mathbf{y}_{k'}^H \mathbf{A}_{1,k}$ by $\mathbf{a}_{k'}^H \mathbf{A}_{1,k}$ amounts to subtracting a linear combination of the first $k' - 1$ rows of \mathbf{U}_k from the k' th row of \mathbf{U}_k . This operation does not affect the value of $\det(\mathbf{U}_k)$ [9].

Similarly to what we have done for Δ_k , we will next show that $\tilde{\mathbf{q}}_k$ can be expressed in terms of $\mathbf{A}_{1,k}$ only. We start by noting that, since \mathbf{V}_k is nonsingular, we can rewrite (22) as

$$[\mathbf{y}_1 \ \mathbf{y}_2 \ \cdots \ \mathbf{y}_k] = [\mathbf{a}_1 \ \mathbf{a}_2 \ \cdots \ \mathbf{a}_k] \mathbf{V}_k^{-1}. \quad (28)$$

Next, from $\mathbf{V}_k = \mathbf{D}_k^{-1} \mathbf{U}_k$ we obtain that

$$\mathbf{V}_k^{-1} = \mathbf{U}_k^{-1} \mathbf{D}_k = \frac{\text{adj}(\mathbf{U}_k)}{\det(\mathbf{U}_k)} \mathbf{D}_k$$

and hence, by (24), that

$$\mathbf{V}_k^{-1} = \frac{1}{\Delta_k} \underbrace{\begin{bmatrix} \Gamma_{1,1}^{(k)} & \Gamma_{2,1}^{(k)} & \cdots & \Gamma_{k,1}^{(k)} \\ 0 & \Gamma_{2,2}^{(k)} & \cdots & \Gamma_{k,2}^{(k)} \\ \vdots & \vdots & \ddots & \vdots \\ 0 & 0 & \cdots & \Gamma_{k,k}^{(k)} \end{bmatrix}}_{\text{adj}(\mathbf{U}_k)} \mathbf{D}_k \quad (29)$$

where $\text{adj}(\mathbf{U}_k)$ is upper triangular since \mathbf{U}_k is upper triangular, and $\Gamma_{n,m}^{(k)}$ denotes the cofactor of \mathbf{U}_k relative to the matrix entry $[\mathbf{U}_k]_{n,m}$ ($n = 1, 2, \dots, k$; $m = n, n+1, \dots, k$) [9]. Note that in order to handle the case $k = 1$ correctly, for which $\text{adj}(\mathbf{U}_1) = \Gamma_{1,1}^{(1)}$, $\det(\mathbf{U}_1) = \mathbf{U}_1 = \Delta_1$, and $\mathbf{U}_1^{-1} = 1/\Delta_1$, we define $\Gamma_{1,1}^{(1)} \triangleq 1$. From (28) and (29) it follows that

$$\begin{aligned} \mathbf{y}_k &= \frac{1}{\Delta_k} \mathbf{y}_k^H \mathbf{y}_k \sum_{i=1}^k \Gamma_{k,i}^{(k)} \mathbf{a}_i \\ &= \frac{1}{\Delta_{k-1}} \sum_{i=1}^k \Gamma_{k,i}^{(k)} \mathbf{a}_i \end{aligned}$$

and therefore, by (18), we get

$$\tilde{\mathbf{q}}_k = \sum_{i=1}^k \Gamma_{k,i}^{(k)} \mathbf{a}_i \quad (30)$$

which evaluates to $\tilde{\mathbf{q}}_1 = \mathbf{a}_1$ for $k = 1$. Next, for $k > 1$ we denote by $\mathbf{A}_{1,k \setminus i}$ the matrix obtained by removing the i th column of $\mathbf{A}_{1,k}$, and we express $\Gamma_{k,i}^{(k)}$ as a function of $\mathbf{a}_1, \mathbf{a}_2, \dots, \mathbf{a}_k$ according to

$$\begin{aligned} \Gamma_{k,i}^{(k)} &= (-1)^{k+i} \det \begin{bmatrix} \mathbf{y}_1^H \mathbf{A}_{1,k \setminus i} \\ \mathbf{y}_2^H \mathbf{A}_{1,k \setminus i} \\ \vdots \\ \mathbf{y}_{k-1}^H \mathbf{A}_{1,k \setminus i} \end{bmatrix} \\ &= (-1)^{k+i} \det(\mathbf{A}_{1,k-1}^H \mathbf{A}_{1,k \setminus i}) \end{aligned}$$

where the last equality is derived analogously to (26) and (27). Thus, (30) can be written as

$$\tilde{\mathbf{q}}_k = \begin{cases} \mathbf{a}_k, & k = 1 \\ \sum_{i=1}^k (-1)^{k+i} \det(\mathbf{A}_{1,k-1}^H \mathbf{A}_{1,k \setminus i}) \mathbf{a}_i, & k > 1. \end{cases} \quad (31)$$

Finally, we obtain

$$\tilde{\mathbf{r}}_k^T = \tilde{\mathbf{q}}_k^H \mathbf{A} \quad (32)$$

as implied by (3), (11), and (12). The results of Step 1a are the relations (27), (31), and (32), which are valid for $(K, k) \in \mathcal{K}_1$.

Step 1b. We next show that (27), (31), and (32) hold for $(K, k) \in \mathcal{K}_2$ as well. Throughout Step 1b we assume that $(K, k) \in \mathcal{K}_2$, and, unless specified otherwise, all equations and statements involving k are valid for $k = K + 1, K + 2, \dots, M$. We know from Section 4.1 that $[\mathbf{R}]_{K+1, K+1} = \mathbf{0}$. According to the definition of \mathcal{M} , $[\mathbf{R}]_{K+1, K+1} = \mathbf{0}$ implies $\Delta_k = 0$, $\tilde{\mathbf{q}}_k = \mathbf{0}$, and $\tilde{\mathbf{r}}_k^T = \mathbf{0}$. It is therefore to be shown that the RHS of (27) evaluates to zero, and that the RHS expressions of (31) and (32) evaluate to all-zero vectors. We start by noting that since $k > K$, $\mathbf{A}_{1,k}$ is rank-deficient. Since $\text{rank}(\mathbf{A}_{1,k}^H \mathbf{A}_{1,k}) = \text{rank}(\mathbf{A}_{1,k}) < k$, we obtain that $\det(\mathbf{A}_{1,k}^H \mathbf{A}_{1,k})$ on the RHS of (27) evaluates to zero. Next, for $k > \max(K, 1)$, the expression

$$\sum_{i=1}^k (-1)^{k+i} \det(\mathbf{A}_{1,k-1}^H \mathbf{A}_{1,k \setminus i}) \mathbf{a}_i \quad (33)$$

on the RHS of (31) is a vector whose p th component can be written, by inverse Laplace expansion [9], as

$$\sum_{i=1}^k (-1)^{k+i} \det(\mathbf{A}_{1,k-1}^H \mathbf{A}_{1,k \setminus i}) [\mathbf{A}]_{p,i} = \det \begin{bmatrix} \mathbf{A}_{1,k-1}^H \mathbf{a}_1 & \mathbf{A}_{1,k-1}^H \mathbf{a}_2 & \cdots & \mathbf{A}_{1,k-1}^H \mathbf{a}_k \\ [\mathbf{A}]_{p,1} & [\mathbf{A}]_{p,2} & \cdots & [\mathbf{A}]_{p,k} \end{bmatrix} \quad (34)$$

for all $p = 1, 2, \dots, P$. Now, again for $k > \max(K, 1)$, since $\mathbf{A}_{1,k}$ is rank-deficient, \mathbf{a}_k can be written as a linear combination

$$\mathbf{a}_k = \sum_{k'=1}^{k-1} \beta^{(k')} \mathbf{a}_{k'}$$

(for some coefficients $\beta^{(k')}$, $k' = 1, 2, \dots, k-1$) which implies that, for all $p = 1, 2, \dots, P$, the argument of the determinant on the RHS of (34) has

$$\begin{bmatrix} \mathbf{A}_{1,k-1}^H \mathbf{a}_k \\ [\mathbf{A}]_{p,k} \end{bmatrix} = \sum_{k'=1}^{k-1} \beta^{(k')} \begin{bmatrix} \mathbf{A}_{1,k-1}^H \mathbf{a}_{k'} \\ [\mathbf{A}]_{p,k'} \end{bmatrix}$$

as its last column. Since this column is a linear combination of the first $k-1$ columns, the determinant on the RHS of (34) is equal to zero for all $p = 1, 2, \dots, P$, and hence the expression in (33) is equal to an all-zero vector for $k > \max(K, 1)$. Moreover, if $K = 0$ and $k = 1$, we have $\mathbf{a}_1 = \mathbf{0}$ on the RHS of (31). Hence, the RHS of (31) evaluates to an all-zero vector for all $(K, k) \in \mathcal{K}_2$. Thus, (31) simplifies to $\tilde{\mathbf{q}}_k = \mathbf{0}$, which in turn implies that the RHS of (32) evaluates to an all-zero vector as well. We have therefore shown that (27), (31), and (32) hold for $(K, k) \in \mathcal{K}_2$. Finally, since $\mathcal{K}_1 \cup \mathcal{K}_2 = \mathcal{K}$, the results of Steps 1a and 1b imply that (27), (31), and (32) are valid for $(K, k) \in \mathcal{K}$.

Step 2. We note that the derivations presented in Steps 1a and 1b for a given $s_0 \in \mathcal{U}$ do not depend on s_0 and can hence be carried over to all $s_0 \in \mathcal{U}$. Thus, we can rewrite (27), (31), and (32), respectively, as

$$\Delta_k(s) = \det(\mathbf{A}_{1,k}^H(s)\mathbf{A}_{1,k}(s)) \quad (35)$$

$$\tilde{\mathbf{q}}_k(s) = \begin{cases} \mathbf{a}_k(s), & k = 1 \\ \sum_{i=1}^k (-1)^{k+i} \det(\mathbf{A}_{1,k-1}^H(s)\mathbf{A}_{1,k \setminus i}(s))\mathbf{a}_i(s), & k > 1 \end{cases} \quad (36)$$

$$\tilde{\mathbf{r}}_k^T(s) = \tilde{\mathbf{q}}_k^H(s)\mathbf{A}(s) \quad (37)$$

for $k = 1, 2, \dots, M$ and $s \in \mathcal{U}$.

Step 3. For $k = 1, 2, \dots, M$, we note that $\mathbf{A}(s) \sim (V_1, V_2)$, along with $V = V_1 + V_2$, implies $\mathbf{A}_{1,k}^H(s)\mathbf{A}_{1,k}(s) \sim (V, V)$. Now, the determinant on the RHS of (35) can be expressed through Laplace expansion as a sum of products of k entries of $\mathbf{A}_{1,k}^H(s)\mathbf{A}_{1,k}(s) \sim (V, V)$. Therefore, we get $\Delta_k(s) \sim (kV, kV)$ for $k = 1, 2, \dots, M$. Analogously, for $k = 2, 3, \dots, M$ we obtain $\det(\mathbf{A}_{1,k-1}^H(s)\mathbf{A}_{1,k \setminus i}(s)) \sim ((k-1)V, (k-1)V)$. The latter result, combined with $\mathbf{A}(s) \sim (V_1, V_2)$ in (36) yields $\tilde{\mathbf{q}}_k(s) \sim ((k-1)V + V_1, (k-1)V + V_2)$, which holds for $k = 1$ as well as a trivial consequence of (36) and $\mathbf{A}(s) \sim (V_1, V_2)$. Finally, from $\tilde{\mathbf{q}}_k(s) \sim ((k-1)V + V_1, (k-1)V + V_2)$ and (37), using $\mathbf{A}(s) \sim (V_1, V_2)$ and $V = V_1 + V_2$, we obtain $\tilde{\mathbf{r}}_k^T(s) \sim (kV, kV)$ for $k = 1, 2, \dots, M$. \square

5. Application to MIMO-OFDM

We are now ready to show how the results derived in the previous section lead to algorithms that exploit the polynomial nature of the MIMO channel transfer function $\mathbf{H}(s) \sim (0, L)$ to perform efficient interpolation-based computation of QR factors of $\mathbf{H}(s_n)$, for all $n \in \mathcal{D}$, given knowledge of $\mathbf{H}(s_n)$ for $n \in \mathcal{E}$. We note that the algorithms described in the following apply to QR decomposition of generic polynomial matrices that are oversampled on the unit circle.

Within the algorithms to be presented, interpolation involves base points and target points on \mathcal{U} that correspond to OFDM tones indexed by integers taken from the set $\{0, 1, \dots, N-1\}$. For a given set $\mathcal{X} \subseteq \{0, 1, \dots, N-1\}$ of OFDM tones, we define $\mathcal{S}(\mathcal{X}) \triangleq \{s_n : n \in \mathcal{X}\}$ to denote the set of corresponding points on \mathcal{U} . With this definition in place, we start by summarizing the brute-force approach described in Section 3.3.

Algorithm 1: Brute-force per-tone QR decomposition

1. Interpolate $\mathbf{H}(s)$ from $\mathcal{S}(\mathcal{E})$ to $\mathcal{S}(\mathcal{D})$.
2. For each $n \in \mathcal{D}$, perform QR decomposition on $\mathbf{H}(s_n)$ to obtain $\mathbf{Q}(s_n)$ and $\mathbf{R}(s_n)$.

It is obvious that for large D , performing QR decomposition on a per-tone basis will result in high computational complexity. However, in the practically relevant case $L \ll D$ the OFDM system effectively

highly oversamples the MIMO channel's transfer function, so that $\mathbf{H}(s_n)$ changes slowly across n . This observation, combined with the results in Section 4, constitutes the basis for a new class of algorithms that perform QR decomposition at a small number of tones and obtain the remaining QR factors through interpolation. More specifically, the basic idea of interpolation-based QR decomposition is as follows. By applying Theorem 9 to the $M_R \times M_T$ LP matrix $\mathbf{H}(s) \sim (0, L)$, we obtain $\tilde{\mathbf{q}}_k(s) \sim ((k-1)L, kL)$ and $\tilde{\mathbf{r}}_k^T(s) \sim (kL, kL)$ for $k = 1, 2, \dots, M_T$. In order to simplify the exposition, in the remainder of the paper we consider $\tilde{\mathbf{q}}_k(s)$ as satisfying $\tilde{\mathbf{q}}_k(s) \sim (kL, kL)$. The resulting statements

$$\tilde{\mathbf{q}}_k(s), \tilde{\mathbf{r}}_k^T(s) \sim (kL, kL), \quad k = 1, 2, \dots, M_T \quad (38)$$

imply that both $\tilde{\mathbf{q}}_k(s)$ and $\tilde{\mathbf{r}}_k^T(s)$ can be interpolated from at least $2kL + 1$ base points, and that, as a consequence of $V_1 = V_2 = kL$, the corresponding interpolation matrices are real-valued. For $k = 1, 2, \dots, M_T$, the interpolation-based algorithms to be presented compute $\tilde{\mathbf{q}}_k(s_n)$ and $\tilde{\mathbf{r}}_k^T(s_n)$, through QR decomposition followed by application of the mapping \mathcal{M} , at a subset of OFDM tones of cardinality at least $2kL + 1$, then interpolate $\tilde{\mathbf{q}}_k(s)$ and $\tilde{\mathbf{r}}_k^T(s)$ to obtain $\tilde{\mathbf{q}}_k(s_n)$ and $\tilde{\mathbf{r}}_k^T(s_n)$ at the remaining tones, and finally apply the inverse mapping \mathcal{M}^{-1} at these tones. In the following, the sets $\mathcal{I}_k \subseteq \{0, 1, \dots, N-1\}$, with $\mathcal{I}_{k-1} \subseteq \mathcal{I}_k$ and $B_k \triangleq |\mathcal{I}_k| \geq 2kL + 1$ ($k = 1, 2, \dots, M_T$), contain the indices corresponding to the OFDM tones chosen as base points. For completeness, we define $\mathcal{I}_0 \triangleq \emptyset$. Specific choices of the sets \mathcal{I}_k will be discussed in detail in Section 8.

We start with a conceptually simple algorithm for interpolation-based QR decomposition, derived from the observation that the M_T statements in (38) can be unified into the single statement $\tilde{\mathbf{Q}}(s), \tilde{\mathbf{R}}(s) \sim (M_T L, M_T L)$. This implies that we can interpolate $\tilde{\mathbf{Q}}(s)$ and $\tilde{\mathbf{R}}(s)$ from a single set of base points of cardinality B_{M_T} . The corresponding algorithm can be formulated as follows:

Algorithm II: Single interpolation step

1. Interpolate $\mathbf{H}(s)$ from $\mathcal{S}(\mathcal{E})$ to $\mathcal{S}(\mathcal{I}_{M_T})$.
2. For each $n \in \mathcal{I}_{M_T}$, perform QR decomposition on $\mathbf{H}(s_n)$ to obtain $\mathbf{Q}(s_n)$ and $\mathbf{R}(s_n)$.
3. For each $n \in \mathcal{I}_{M_T}$, apply $\mathcal{M} : (\mathbf{Q}(s_n), \mathbf{R}(s_n)) \mapsto (\tilde{\mathbf{Q}}(s_n), \tilde{\mathbf{R}}(s_n))$.
4. Interpolate $\tilde{\mathbf{Q}}(s)$ and $\tilde{\mathbf{R}}(s)$ from $\mathcal{S}(\mathcal{I}_{M_T})$ to $\mathcal{S}(\mathcal{D} \setminus \mathcal{I}_{M_T})$.
5. For each $n \in \mathcal{D} \setminus \mathcal{I}_{M_T}$, apply $\mathcal{M}^{-1} : (\tilde{\mathbf{Q}}(s_n), \tilde{\mathbf{R}}(s_n)) \mapsto (\mathbf{Q}(s_n), \mathbf{R}(s_n))$.

This formulation of Algorithm II assumes that $\mathbf{H}(s_n)$ has full rank for all $n \in \mathcal{D} \setminus \mathcal{I}_{M_T}$, which allows to perform all inverse mappings \mathcal{M}^{-1} in Step 5 using (13)–(15) only. If, however, for a given $n \in \mathcal{D} \setminus \mathcal{I}_{M_T}$, $\mathbf{H}(s_n)$ is rank-deficient with ordered column rank $K < M_T$, we have $\tilde{\mathbf{Q}}_{K+1, M_T}(s_n) = \mathbf{0}$ and $\tilde{\mathbf{R}}^{K+1, M_T}(s_n) = \mathbf{0}$. Hence, according to the results in Section 4.2, $\mathbf{Q}_{K+1, M_T}(s_n)$ and $\mathbf{R}^{K+1, M_T}(s_n)$ must be computed through QR decomposition of $\mathbf{H}_{K+1, M_T}(s_n) - \mathbf{Q}_{1, K}(s_n) \mathbf{R}_{K+1, M_T}^{1, K}(s_n)$ for $K > 0$ or of $\mathbf{H}(s_n)$ for $K = 0$. This, in turn, requires $\mathbf{H}_{K+1, M_T}(s_n)$ to be obtained by interpolating $\mathbf{H}_{K+1, M_T}(s)$ from $\mathcal{S}(\mathcal{E})$ to the single target

point s_n in an additional step. For simplicity of exposition, in the remainder of the paper we will assume that $\mathbf{H}(s_n)$ is full-rank for all $n \in \mathcal{D}$.

Departing from Algorithm II, which interpolates $\tilde{\mathbf{q}}_k(s)$ and $\tilde{\mathbf{r}}_k^T(s)$ from B_{M_T} base points, we next present a more sophisticated algorithm that involves interpolation of $\tilde{\mathbf{q}}_k(s)$ and $\tilde{\mathbf{r}}_k^T(s)$ from $B_k \leq B_{M_T}$ base points ($k = 1, 2, \dots, M_T$), in agreement with (38). The resulting Algorithm III consists of M_T iterations. In the first iteration, the tones $n \in \mathcal{I}_1$ are considered. At each of these tones, QR decomposition is performed on $\mathbf{H}(s_n)$, resulting in $\mathbf{Q}(s_n)$ and $\mathbf{R}(s_n)$, which are then mapped to $(\tilde{\mathbf{Q}}(s_n), \tilde{\mathbf{R}}(s_n))$ by applying \mathcal{M} . Next, $\tilde{\mathbf{q}}_1(s)$ and $\tilde{\mathbf{r}}_1^T(s)$ are interpolated from the tones $n \in \mathcal{I}_1$ to the remaining tones $n \in \mathcal{D} \setminus \mathcal{I}_1$. In the k th iteration ($k = 2, 3, \dots, M_T$), the tones $n \in \mathcal{I}_k \setminus \mathcal{I}_{k-1}$ are considered. At each of these tones, $\mathbf{Q}_{1,k-1}(s_n)$ and $\mathbf{R}^{1,k-1}(s_n)$ are obtained² by applying \mathcal{M}^{-1} to $(\tilde{\mathbf{Q}}_{1,k-1}(s_n), \tilde{\mathbf{R}}^{1,k-1}(s_n))$, already known from the previous iterations, whereas the submatrices $\mathbf{Q}_{k,M_T}(s_n)$ and $\mathbf{R}_{k,M_T}^{k,M_T}(s_n)$ are obtained by performing QR decomposition on the matrix $\mathbf{H}_{k,M_T}(s_n) - \mathbf{Q}_{1,k-1}(s_n)\mathbf{R}_{k,M_T}^{1,k-1}(s_n)$, in accordance with Proposition 6, and $\mathbf{R}^{k,M_T}(s_n)$ is given, for $k > 1$, by $[\mathbf{0} \quad \mathbf{R}_{k,M_T}^{k,M_T}(s_n)]$. Next, the submatrices $\tilde{\mathbf{Q}}_{k,M_T}(s_n)$ and $\tilde{\mathbf{R}}^{k,M_T}(s_n)$ are computed by applying \mathcal{M} to $(\mathbf{Q}_{k,M_T}(s_n), \mathbf{R}_{k,M_T}^{k,M_T}(s_n))$. Since the samples $\tilde{\mathbf{q}}_k(s_n)$ and $\tilde{\mathbf{r}}_k^T(s_n)$ are now known at all tones $n \in \mathcal{I}_k$, $\tilde{\mathbf{q}}_k(s)$ and $\tilde{\mathbf{r}}_k^T(s)$ can be interpolated from the tones $n \in \mathcal{I}_k$ to the remaining tones $n \in \mathcal{D} \setminus \mathcal{I}_k$, thereby completing the k th iteration. After M_T iterations, we know $\tilde{\mathbf{Q}}(s_n)$ and $\tilde{\mathbf{R}}(s_n)$ at all tones $n \in \mathcal{D}$, as well as $\mathbf{Q}(s_n)$ and $\mathbf{R}(s_n)$ at the tones $n \in \mathcal{I}_{M_T}$. The last step consists of applying \mathcal{M}^{-1} to $(\tilde{\mathbf{Q}}(s_n), \tilde{\mathbf{R}}(s_n))$ to obtain $\mathbf{Q}(s_n)$ and $\mathbf{R}(s_n)$ at the remaining tones $n \in \mathcal{D} \setminus \mathcal{I}_k$. The algorithm is formulated as follows:

Algorithm III: Multiple interpolation steps

1. Set $k \leftarrow 1$.
2. Interpolate $\mathbf{H}_{k,M_T}(s)$ from $\mathcal{S}(\mathcal{E})$ to $\mathcal{S}(\mathcal{I}_k \setminus \mathcal{I}_{k-1})$.
3. If $k = 1$, go to Step 5. Otherwise, for each $n \in \mathcal{I}_k \setminus \mathcal{I}_{k-1}$, apply $\mathcal{M}^{-1} : (\tilde{\mathbf{Q}}_{1,k-1}(s_n), \tilde{\mathbf{R}}^{1,k-1}(s_n)) \mapsto (\mathbf{Q}_{1,k-1}(s_n), \mathbf{R}^{1,k-1}(s_n))$.
4. For each $n \in \mathcal{I}_k \setminus \mathcal{I}_{k-1}$, overwrite $\mathbf{H}_{k,M_T}(s_n)$ by $\mathbf{H}_{k,M_T}(s_n) - \mathbf{Q}_{1,k-1}(s_n)\mathbf{R}_{k,M_T}^{1,k-1}(s_n)$.
5. For each $n \in \mathcal{I}_k \setminus \mathcal{I}_{k-1}$, perform QR decomposition on $\mathbf{H}_{k,M_T}(s_n)$ to obtain $\mathbf{Q}_{k,M_T}(s_n)$ and $\mathbf{R}_{k,M_T}^{k,M_T}(s_n)$, and, if $k > 1$, construct $\mathbf{R}^{k,M_T}(s_n) = [\mathbf{0} \quad \mathbf{R}_{k,M_T}^{k,M_T}(s_n)]$.
6. For each $n \in \mathcal{I}_k \setminus \mathcal{I}_{k-1}$, apply $\mathcal{M} : (\mathbf{Q}_{k,M_T}(s_n), \mathbf{R}_{k,M_T}^{k,M_T}(s_n)) \mapsto (\tilde{\mathbf{Q}}_{k,M_T}(s_n), \tilde{\mathbf{R}}^{k,M_T}(s_n))$.
7. Interpolate $\tilde{\mathbf{q}}_k(s)$ and $\tilde{\mathbf{r}}_k^T(s)$ from $\mathcal{S}(\mathcal{I}_k)$ to $\mathcal{S}(\mathcal{D} \setminus \mathcal{I}_k)$.
8. If $k = M_T$, proceed to the next step. Otherwise, set $k \leftarrow k + 1$ and go back to Step 2.
9. For each $n \in \mathcal{D} \setminus \mathcal{I}_{M_T}$, apply $\mathcal{M}^{-1} : (\tilde{\mathbf{Q}}(s_n), \tilde{\mathbf{R}}(s_n)) \mapsto (\mathbf{Q}(s_n), \mathbf{R}(s_n))$.

In comparison with Algorithm II, Algorithm III performs QR decompositions on increasingly smaller matrices. The corresponding computational complexity savings are, however, traded against an increase in

²The mapping \mathcal{M} and its inverse \mathcal{M}^{-1} are defined on submatrices of $\mathbf{Q}(s_n)$ and $\mathbf{R}(s_n)$ according to (10)–(15).

interpolation effort and the computational overhead associated with Step 4, which will be referred to as the *reduction step* in what follows. Moreover, the complexity of applying \mathcal{M} and \mathcal{M}^{-1} differs for the two algorithms. A detailed complexity analysis provided in the next section will show that, depending on the system parameters, Algorithm III can exhibit smaller complexity than Algorithm II.

We conclude this section with some remarks on ordered SC MIMO-OFDM detectors [13], which essentially permute the columns of $\mathbf{H}(s_n)$ to perform SC detection of the transmitted data symbols according to a given sorting criterion (such as, e.g., V-BLAST sorting [21]) to obtain better detection performance than in the unsorted case. The permutation of the columns of $\mathbf{H}(s_n)$ can be represented by means of right-multiplication of $\mathbf{H}(s_n)$ by an $M_T \times M_T$ permutation matrix $\mathbf{P}(s_n)$. The matrices subjected to QR decomposition are then given by $\mathbf{H}(s_n)\mathbf{P}(s_n), n \in \mathcal{D}$. If $\mathbf{P}(s_n)$ is constant across all OFDM tones, i.e., $\mathbf{P}(s_n) = \mathbf{P}_0, n \in \mathcal{D}$, we have $\mathbf{H}(s)\mathbf{P}_0 \sim (0, L)$ and Algorithms I–III can be applied to $\mathbf{H}(s_n)\mathbf{P}_0$. A MIMO-OFDM ordered SC detector using Algorithm II to compute QR factors of $\mathbf{H}(s)\mathbf{P}_0$, along with a strategy for choosing \mathbf{P}_0 , was presented in [22]. If $\mathbf{P}(s_n)$ varies across n , the matrices $\mathbf{H}(s_n)\mathbf{P}(s_n), n \in \mathcal{D}$, in general, can no longer be seen as samples of a polynomial matrix of maximum degree $L \ll D$, so that the interpolation-based QR decomposition algorithms presented above can not be applied.

6. Complexity Analysis

We are next interested in assessing under which circumstances the interpolation-based Algorithms II and III offer computational complexity savings over the brute-force approach in Algorithm I. To this end, we propose a simple computational complexity metric, representative of VLSI circuit complexity as quantified by the product of chip area and processing delay [10]. We note that other important aspects of VLSI design, including, e.g., wordwidth requirements, memory access strategies, and datapath architecture, are not accounted for in our analysis. Nevertheless, the proposed metric is indicative of the complexity of Algorithms I–III and allows to quantify the impact of the system parameters on the potential savings of interpolation-based QR decomposition over brute-force per-tone QR decomposition.

In the remainder of the paper, unless explicitly specified otherwise, the term *complexity* refers to computational complexity according to the metric defined in Section 6.1 below. We derive the complexity of individual *computational tasks* (i.e., interpolation, QR decomposition, mapping \mathcal{M} , inverse mapping \mathcal{M}^{-1} , and reduction step) in Section 6.2. Then, we proceed to computing the total complexity of Algorithms I–III in Section 6.3. Finally, in Section 6.4 we compare the complexity results obtained in Section 6.3 and we derive conditions on the system parameters under which Algorithms II and III exhibit lower complexity than Algorithm I.

6.1. Complexity Metric

In the VLSI implementation of a given algorithm, a wide range of trade-offs between silicon area A and processing delay τ can, in general, be realized [10]. Parallel processing reduces τ at the expense of a larger A , whereas resource sharing reduces A at the expense of a larger τ . However, the corresponding circuit transformations typically do not affect the area-delay product $A\tau$ significantly. For this reason, the area-delay product is considered a relevant indicator of algorithm complexity [10]. In the definition of the specific complexity metric that will be used subsequently, we only take into account the arithmetic operations with a significant impact on $A\tau$. More specifically, we divide the operations underlying the algorithms under consideration into three classes, namely i) multiplications, ii) divisions and square roots, and iii) additions and subtractions. Class iii) operations will not be counted as they typically have a significantly lower VLSI circuit complexity than Class i) and Class ii) operations.

In all algorithms presented in this paper, the number of Class i) operations is significantly larger than the number of Class ii) operations.³ By assuming a VLSI architecture where the Class ii) operations are performed by low-area high-delay arithmetical units operating in parallel to the multipliers performing the Class i) operations, it follows that the Class i) operations dominate the overall complexity and the Class ii) operations can be neglected.

Within Class i), we distinguish between *full multiplications* (i.e., multiplications of two variable operands) and *constant multiplications* (i.e., multiplications of a variable operand by a constant operand⁴). We define the cost of a full multiplication as the unit of computational complexity. We do not distinguish between real-valued full multiplications and complex-valued full multiplications, as we assume that both are performed by multipliers designed to process two variable complex-valued operands. The fact, discussed in detail in Section 8.1, that a constant multiplication can be implemented in VLSI at significantly smaller cost than a full multiplication, will be accounted for through a weighting factor smaller than one.

6.2. Per-Tone Complexity of Individual Computational Tasks

In order to simplify the notation, in the remainder of this section we drop the dependence of all quantities on s_n . We furthermore introduce the auxiliary variable

$$J_k \triangleq M_R k + M_T k - \frac{(k-1)k}{2}, \quad k = 1, 2, \dots, M_T$$

³We assume that division of an M -dimensional vector \mathbf{a} by a scalar α , such as the divisions in (2), (13), or (14), is implemented by first computing the single division $\beta \triangleq 1/\alpha$ and then multiplying the M entries of \mathbf{a} by β , at the cost of one Class ii) operation and M Class i) operations, respectively.

⁴In the context of the interpolation-based algorithms considered in this paper, all operands that depend on $\mathbf{H}(s)$ are assumed variable. The coefficients of interpolation filters, e.g., are treated as constant operands. For a detailed discussion on the difference between full multiplications and constant multiplications, we refer to Section 8.1.

which specifies the maximum total number of nonzero entries in $\mathbf{Q}_{1,k}$ and $\mathbf{R}^{1,k}$, and hence also in $\tilde{\mathbf{Q}}_{1,k}$ and $\tilde{\mathbf{R}}^{1,k}$, in accordance with the fact that \mathbf{R} and $\tilde{\mathbf{R}}$ are upper triangular.

Interpolation. We quantify the complexity of interpolating an LP to one target point through an equivalent of c_{IP} full multiplications. The dependence of interpolation complexity on the underlying VLSI implementation and on the number of base points is assumed to be incorporated into c_{IP} . Specific strategies for efficient interpolation along with the corresponding values of c_{IP} are presented in Section 8. Since interpolation of an LP matrix is performed entrywise, the complexity of interpolating $\mathbf{H}_{k,M_T}(s)$ to one target point is given by

$$c_{\text{IP},\mathbf{H}}^{k,M_T} = M_R(M_T - k + 1)c_{\text{IP}}, \quad k = 1, 2, \dots, M_T.$$

Similarly, interpolation of $\tilde{\mathbf{Q}}(s)$ and $\tilde{\mathbf{R}}(s)$ to one target point has complexity

$$c_{\text{IP},\tilde{\mathbf{Q}}\tilde{\mathbf{R}}} = J_{M_T}c_{\text{IP}}$$

and the complexity of interpolating $\tilde{\mathbf{q}}_k(s)$ and $\tilde{\mathbf{r}}_k^T(s)$ to one target point is given by

$$c_{\text{IP},\tilde{\mathbf{q}}\tilde{\mathbf{r}}}^{(k)} = (M_R + M_T - k + 1)c_{\text{IP}}, \quad k = 1, 2, \dots, M_T.$$

QR decomposition. In order to keep our discussion independent of the QR decomposition method, we denote the cost of performing QR decomposition on an $M_R \times k$ matrix by $c_{\text{QR}}^{M_R \times k}$ ($k = 1, 2, \dots, M_T$). Specific expressions for $c_{\text{QR}}^{M_R \times k}$ will only be required in the numerical complexity analysis in Section 9.

Mapping \mathcal{M} . We denote the overall cost of mapping $(\mathbf{Q}_{k,M_T}, \mathbf{R}^{k,M_T})$ to $(\tilde{\mathbf{Q}}_{k,M_T}, \tilde{\mathbf{R}}^{k,M_T})$ ($k = 1, 2, \dots, M_T$) by $c_{\mathcal{M}}^{k,M_T}$. In the case $k = 1$, application of the mapping \mathcal{M} requires computation of $[\mathbf{R}]_{1,1}$, $[\mathbf{R}]_{1,1}^2$, $[\mathbf{R}]_{1,1}^2[\mathbf{R}]_{2,2}$, $[\mathbf{R}]_{1,1}^2[\mathbf{R}]_{2,2}^2, \dots, \prod_{i=1}^{M_T} [\mathbf{R}]_{i,i}^2$, at the cost of $2M_T - 1$ full multiplications. This step yields both the scaling factors $\Delta_{k'-1}[\mathbf{R}]_{k',k'}$, $k' = 1, 2, \dots, M_T$, and the diagonal entries of $\tilde{\mathbf{R}}$. From (31) we can deduce that the first column of $\tilde{\mathbf{Q}}$ is equal to the first column of \mathbf{H} and is hence obtained at zero complexity. The remaining entries of $\tilde{\mathbf{Q}}$ and the entries of $\tilde{\mathbf{R}}$ above the main diagonal are obtained by scaling the corresponding entries of \mathbf{Q} and \mathbf{R} according to (11) and (12), respectively, which requires $J_{M_T} - M_R - M_T$ full multiplications. Hence, we obtain

$$c_{\mathcal{M}}^{1,M_T} = J_{M_T} - M_R + M_T - 1.$$

Next, we consider the case $k > 1$, which only occurs in Step 3 of Algorithm III, where $\Delta_{k-1} = [\tilde{\mathbf{R}}]_{k-1,k-1}$ is already available from the previous iteration which involves interpolation of $\tilde{\mathbf{r}}_{k-1}^T(s)$. The application of the mapping \mathcal{M} first requires computation of $\Delta_{k-1}[\mathbf{R}]_{k,k}$, $\Delta_{k-1}[\mathbf{R}]_{k,k}^2$, $\Delta_{k-1}[\mathbf{R}]_{k,k}^2[\mathbf{R}]_{k+1,k+1}, \dots$, $\Delta_{k-1} \prod_{i=k}^{M_T} [\mathbf{R}]_{i,i}^2$, at the cost of $2(M_T - k + 1)$ full multiplications. Then, the entries of \mathbf{Q}_{k,M_T} and the entries of \mathbf{R}^{k,M_T} above the main diagonal of \mathbf{R} are scaled according to (11) and (12), which requires $J_{M_T} - J_{k-1} - (M_T - k + 1)$ full multiplications. In summary, we obtain

$$c_{\mathcal{M}}^{k,M_T} = J_{M_T} - J_{k-1} + M_T - k + 1, \quad k = 2, 3, \dots, M_T.$$

Table 1: Total complexity associated with the individual computational tasks

Computational task	Symbol ^a	Algorithm I	Algorithm II	Algorithm III
Interpolation of $\mathbf{H}(s)$	$c_{\text{IP},\mathbf{H},A}$	$Dc_{\text{IP},\mathbf{H}}^{1,M_T}$	$B_{M_T}c_{\text{IP},\mathbf{H}}^{1,M_T}$	$B_1c_{\text{IP},\mathbf{H}}^{1,M_T} + 2L \sum_{k=2}^{M_T} c_{\text{IP},\mathbf{H}}^{k,M_T}$
Interpolation of $\tilde{\mathbf{Q}}(s)$ and $\tilde{\mathbf{R}}(s)$	$c_{\text{IP},\tilde{\mathbf{Q}},\tilde{\mathbf{R}},A}$	0	$(D - B_{M_T})c_{\text{IP},\tilde{\mathbf{Q}},\tilde{\mathbf{R}}}$	$\sum_{k=1}^{M_T} (D - B_k)c_{\text{IP},\tilde{\mathbf{q}},\tilde{\mathbf{r}}}^{(k)}$
QR decomposition	$c_{\text{QR},A}$	$Dc_{\text{QR}}^{M_R \times M_T}$	$B_{M_T}c_{\text{QR}}^{M_R \times M_T}$	$B_1c_{\text{QR}}^{M_R \times M_T} + 2L \sum_{k=2}^{M_T} c_{\text{QR}}^{M_R \times (M_T - k + 1)}$
Mapping \mathcal{M}	$c_{\mathcal{M},A}$	0	$B_{M_T}c_{\mathcal{M}}^{1,M_T}$	$B_1c_{\mathcal{M}}^{1,M_T} + 2L \sum_{k=2}^{M_T} c_{\mathcal{M}}^{k,M_T}$
Inverse mapping \mathcal{M}^{-1}	$c_{\mathcal{M}^{-1},A}$	0	$(D - B_{M_T})c_{\mathcal{M}^{-1}}^{1,M_T}$	$2L \sum_{k=2}^{M_T} c_{\mathcal{M}^{-1}}^{1,k-1} + (D - B_{M_T})c_{\mathcal{M}^{-1}}^{1,M_T}$
Reduction	$c_{\text{red},A}$	0	0	$2L \sum_{k=2}^{M_T} c_{\text{red}}^{(k)}$

^a The index A is a placeholder for the algorithm number (I, II, or III).

Inverse mapping \mathcal{M}^{-1} . We denote the overall cost of mapping $(\tilde{\mathbf{Q}}_{1,k}, \tilde{\mathbf{R}}^{1,k})$ to $(\mathbf{Q}_{1,k}, \mathbf{R}^{1,k})$ ($k = 1, 2, \dots, M_T$) by $c_{\mathcal{M}^{-1}}^{1,k}$. Since $\Delta_0 = 1$ and $[\tilde{\mathbf{R}}]_{1,1} = [\mathbf{R}]_{1,1}^2$, by first computing $([\tilde{\mathbf{R}}]_{1,1})^{1/2}$ and then its inverse, we can obtain both $[\mathbf{R}]_{1,1}$ and the scaling factor $(\Delta_0[\mathbf{R}]_{1,1})^{-1} = 1/[\mathbf{R}]_{1,1}$ at the cost of one square root operation and one division. For $k' = 2, 3, \dots, k$, the scaling factors $(\Delta_{k'-1}[\mathbf{R}]_{k',k'})^{-1}$ can be obtained according to (15) by computing $([\tilde{\mathbf{R}}]_{k'-1,k'-1}[\tilde{\mathbf{R}}]_{k',k'})^{-1/2}$, at the cost of $k - 1$ full multiplications, $k - 1$ square root operations, and $k - 1$ divisions. The entries of $\mathbf{Q}_{1,k}$ and the remaining entries of $\mathbf{R}^{1,k}$ on and above the main diagonal of \mathbf{R} are obtained by scaling the corresponding entries of $\tilde{\mathbf{Q}}_{1,k}$ and $\tilde{\mathbf{R}}^{1,k}$ according to (13) and (14), respectively, at the cost of $J_k - 1$ full multiplications. Since we neglect the impact of square root operations and divisions on complexity, we obtain

$$c_{\mathcal{M}^{-1}}^{1,k} = J_k + k - 2, \quad k = 1, 2, \dots, M_T.$$

Reduction step. Since matrix subtraction has negligible complexity, for a given $k \in \{1, 2, \dots, M_T\}$, the complexity associated with the computation of $\mathbf{H}_{k,M_T} - \mathbf{Q}_{1,k-1}\mathbf{R}_{k,M_T}^{1,k-1}$, denoted by $c_{\text{red}}^{(k)}$, is given by the complexity associated with the multiplication of the $M_R \times (k - 1)$ matrix $\mathbf{Q}_{1,k-1}$ by the $(k - 1) \times (M_T - k + 1)$ matrix $\mathbf{R}_{k,M_T}^{1,k-1}$. Hence, we obtain

$$c_{\text{red}}^{(k)} = M_R(k - 1)(M_T - k + 1).$$

6.3. Total Complexity of Algorithms I–III

The contribution of a given computational task to the overall complexity of a given algorithm is obtained by multiplying the corresponding per-tone complexity, computed in the previous section, by the number of

relevant tones. For simplicity of exposition, in the ensuing analysis we restrict ourselves to the case where $B_k = 2kL + 1$ ($k = 1, 2, \dots, M_T$) and $\mathcal{I}_1 \subseteq \mathcal{I}_2 \subseteq \dots \subseteq \mathcal{I}_{M_T} \subset \mathcal{D}$, for which we obtain $|\mathcal{I}_k \setminus \mathcal{I}_{k-1}| = 2L$ and $|\mathcal{D} \setminus \mathcal{I}_k| = D - 2kL - 1$ ($k = 1, 2, \dots, M_T$). With the total complexity of the individual tasks summarized in Table 1, the complexity associated with Algorithms I–III is trivially obtained as

$$C_I = c_{\text{IP},\mathbf{H},\text{I}} + c_{\text{QR},\text{I}} \quad (39)$$

$$C_{\text{II}} = c_{\text{IP},\mathbf{H},\text{II}} + c_{\text{IP},\tilde{\mathbf{Q}}\tilde{\mathbf{R}},\text{II}} + c_{\text{QR},\text{II}} + c_{\mathcal{M},\text{II}} + c_{\mathcal{M}^{-1},\text{II}} \quad (40)$$

$$C_{\text{III}} = c_{\text{IP},\mathbf{H},\text{III}} + c_{\text{IP},\tilde{\mathbf{Q}}\tilde{\mathbf{R}},\text{III}} + c_{\text{QR},\text{III}} + c_{\mathcal{M},\text{III}} + c_{\mathcal{M}^{-1},\text{III}} + c_{\text{red},\text{III}}. \quad (41)$$

6.4. Complexity Comparisons

In the following, we identify conditions on the system parameters and on the interpolation cost c_{IP} that guarantee that Algorithms II and III exhibit smaller complexity than Algorithm I. We start by comparing Algorithms I and II and note that

$$C_I - C_{\text{II}} = (D - B_{M_T}) \left(c_{\text{QR}}^{M_R \times M_T} - c_{\mathcal{M}^{-1}}^{1, M_T} - \frac{M_T (M_T + 1)}{2} c_{\text{IP}} \right) - B_{M_T} c_{\mathcal{M}}^{1, M_T}. \quad (42)$$

Hence, if c_{IP} satisfies

$$c_{\text{IP}} < c_{\text{IP},\text{max},\text{II}} \triangleq \frac{2 \left(c_{\text{QR}}^{M_R \times M_T} - c_{\mathcal{M}^{-1}}^{1, M_T} \right)}{M_T (M_T + 1)} \quad (43)$$

then there exists a D_{min} such that $C_{\text{II}} < C_I$ for $D \geq D_{\text{min}}$, i.e., Algorithm II exhibits a lower complexity than Algorithm I for a sufficiently high number of data-carrying tones D . Moreover, for $c_{\text{IP}} < c_{\text{IP},\text{max},\text{II}}$, increasing B_{M_T} reduces $C_I - C_{\text{II}}$. If the inequality (43) is met, (42) implies, since $B_{M_T} = 2M_T L + 1$, that for increasing L and with all other parameters fixed, Algorithm II exhibits smaller savings. For larger $c_{\text{QR}}^{M_R \times M_T}$, again with all other parameters fixed, Algorithm II exhibits larger savings.

In order to compare Algorithms II and III, we start from (40) and (41) and rewrite $C_{\text{II}} - C_{\text{III}}$ as

$$C_{\text{II}} - C_{\text{III}} = \Delta c_{\text{QR}} + \Delta c_{\mathcal{M},\mathcal{M}^{-1}} + \Delta c_{\text{IP},\mathbf{H}\tilde{\mathbf{Q}}\tilde{\mathbf{R}}} - c_{\text{red},\text{III}} \quad (44)$$

where we have introduced

$$\begin{aligned} \Delta c_{\text{QR}} &\triangleq c_{\text{QR},\text{II}} - c_{\text{QR},\text{III}} \\ \Delta c_{\mathcal{M},\mathcal{M}^{-1}} &\triangleq c_{\mathcal{M},\text{II}} + c_{\mathcal{M}^{-1},\text{II}} - c_{\mathcal{M},\text{III}} - c_{\mathcal{M}^{-1},\text{III}} \\ \Delta c_{\text{IP},\mathbf{H}\tilde{\mathbf{Q}}\tilde{\mathbf{R}}} &\triangleq c_{\text{IP},\mathbf{H},\text{II}} + c_{\text{IP},\tilde{\mathbf{Q}}\tilde{\mathbf{R}},\text{II}} - c_{\text{IP},\mathbf{H},\text{III}} - c_{\text{IP},\tilde{\mathbf{Q}}\tilde{\mathbf{R}},\text{III}}. \end{aligned}$$

From the results in Table 1 we get

$$\Delta c_{\text{QR}} = 2L \sum_{k=2}^{M_T} \left(c_{\text{QR}}^{M_R \times M_T} - c_{\text{QR}}^{M_R \times (M_T - k + 1)} \right) \quad (45)$$

which is positive since, obviously, $c_{\text{QR}}^{M_R \times M_T} > c_{\text{QR}}^{M_R \times (M_T - k + 1)}$ ($k = 2, 3, \dots, M_T$). Furthermore, again employing the results in Table 1, straightforward calculations yield

$$\begin{aligned} \Delta c_{\text{IP}, \mathbf{H}\tilde{\mathbf{Q}}\tilde{\mathbf{R}}} &= -2L \sum_{k=2}^{M_T} k(k-1) c_{\text{IP}} \\ &= -\frac{2}{3} L M_T (M_T^2 - 1) c_{\text{IP}} \end{aligned} \quad (46)$$

and

$$\begin{aligned} \Delta c_{\mathcal{M}, \mathcal{M}^{-1}} &= (B_1 - B_{M_T})(M_R - 1) \\ &= -2L(M_R - 1)(M_T - 1). \end{aligned} \quad (47)$$

We observe that (44)–(47), along with the expression for $c_{\text{red,III}}$ in Table 1, imply that $C_{\text{II}} - C_{\text{III}}$ does not depend on D and is proportional to L . Moreover, it follows from (44) and (46) that $C_{\text{III}} < C_{\text{II}}$ is equivalent to $c_{\text{IP}} < c_{\text{IP}, \text{max,III}}$ with

$$c_{\text{IP}, \text{max,III}} \triangleq \frac{\Delta c_{\text{QR}} + \Delta c_{\mathcal{M}, \mathcal{M}^{-1}} - c_{\text{red,III}}}{\frac{2}{3} L M_T (M_T^2 - 1)}. \quad (48)$$

We note that the RHS of (48) depends solely on M_T and M_R , since Δc_{QR} , $\Delta c_{\mathcal{M}, \mathcal{M}^{-1}}$, and $c_{\text{red,III}}$ are proportional to L . Hence, if $\Delta c_{\text{QR}} + \Delta c_{\mathcal{M}, \mathcal{M}^{-1}} - c_{\text{red,III}} > 0$ and for c_{IP} sufficiently small, Algorithm III has lower complexity than Algorithm II.

7. The MMSE Case

In this section, we modify the QR decomposition algorithms described in Section 5 to obtain corresponding algorithms that compute the MMSE-QR decomposition, as defined in Section 3.2, of the channel matrices $\mathbf{H}(s_n)$, $n \in \mathcal{D}$. In Section 7.1, we discuss the general concept of regularized QR decomposition, of which MMSE-QR decomposition is a special case. In Section 7.2, we use the results of Section 7.1 to formulate and analyze MMSE-QR decomposition algorithms for MIMO-OFDM.

7.1. Regularized QR Decomposition

In the following, we consider, as done in Section 2.2, a generic matrix $\mathbf{A} \in \mathbb{C}^{P \times M}$, with $P \geq M$.

Definition 10. The *regularized QR decomposition* of \mathbf{A} with the real-valued *regularization parameter* $\alpha > 0$, is the unique factorization $\mathbf{A} = \mathbf{Q}\mathbf{R}$, where the *regularized QR factors* $\mathbf{Q} \in \mathbb{C}^{P \times M}$ and $\mathbf{R} \in \mathbb{C}^{M \times M}$ are obtained as follows: $\bar{\mathbf{A}} = \bar{\mathbf{Q}}\mathbf{R}$ is the unique QR decomposition of the full-rank $(P + M) \times M$ augmented matrix $\bar{\mathbf{A}} \triangleq [\mathbf{A}^T \quad \alpha \mathbf{I}_M]^T$, and $\mathbf{Q} \triangleq \bar{\mathbf{Q}}^{1,P}$.

In the following, we consider GS-based and UT-based algorithms for computing the regularized QR decomposition of \mathbf{A} through the QR decomposition of the augmented matrix $\bar{\mathbf{A}}$. We will see that both classes

of algorithms exhibit higher complexity than the corresponding algorithms for QR decomposition of \mathbf{A} described in Section 2.2.

GS-based QR decomposition of $\bar{\mathbf{A}}$ produces \mathbf{Q} , \mathbf{R} , and, as a by-product, the $M \times M$ matrix $\bar{\mathbf{Q}}^{P+1, P+M}$. Since GS-based QR decomposition according to (1)–(3) operates on entire columns of the matrix to be decomposed, the computation of $\bar{\mathbf{Q}}^{P+1, P+M}$ can not be avoided. Thus, GS-based regularized QR decomposition of \mathbf{A} has the same complexity as GS-based QR decomposition of $\bar{\mathbf{A}}$, which in turn has a higher complexity than GS-based QR decomposition of \mathbf{A} .

Representing the UT-based QR decomposition of $\bar{\mathbf{A}}$ in the standard form (4) yields

$$\Theta_U \cdots \Theta_2 \Theta_1 \underbrace{\begin{bmatrix} \mathbf{A} & \mathbf{I}_P & \mathbf{0} \\ \alpha \mathbf{I}_M & \mathbf{0} & \mathbf{I}_M \end{bmatrix}}_{= [\bar{\mathbf{A}} \quad \mathbf{I}_{P+M}]} = \begin{bmatrix} \mathbf{R} & \bar{\mathbf{Q}}^H \\ \mathbf{0} & (\bar{\mathbf{Q}}^\perp)^H \end{bmatrix} \quad (49)$$

with the $(P+M) \times (P+M)$ unitary matrices Θ_u , $u = 1, 2, \dots, U$, and where $\bar{\mathbf{Q}}^\perp$ is a $(P+M) \times P$ matrix satisfying $(\bar{\mathbf{Q}}^\perp)^H \bar{\mathbf{Q}}^\perp = \mathbf{I}_P$ and $\bar{\mathbf{Q}}^H \bar{\mathbf{Q}}^\perp = \mathbf{0}$. By rewriting the RHS of (49) as

$$\begin{bmatrix} \mathbf{R} & \bar{\mathbf{Q}}^H \\ \mathbf{0} & (\bar{\mathbf{Q}}^\perp)^H \end{bmatrix} = \begin{bmatrix} \mathbf{R} & \mathbf{Q}^H & (\bar{\mathbf{Q}}^{P+1, P+M})^H \\ \mathbf{0} & ((\bar{\mathbf{Q}}^\perp)^{1, P})^H & ((\bar{\mathbf{Q}}^\perp)^{P+1, P+M})^H \end{bmatrix} \quad (50)$$

we observe that UT-based regularized QR decomposition of \mathbf{A} according to (49), besides computing \mathbf{R} and \mathbf{Q}^H , yields the matrices $(\bar{\mathbf{Q}}^\perp)^H$ and $(\bar{\mathbf{Q}}^{P+1, P+M})^H$ as by-products. As observed previously in [3], the corresponding complexity overhead can not be eliminated completely, but it can be reduced by removing the last M columns on both sides of (49). Thus, using (50), we obtain the *efficient UT-based regularized QR decomposition* described by the standard form

$$\Theta_U \cdots \Theta_2 \Theta_1 \begin{bmatrix} \mathbf{A} & \mathbf{I}_P \\ \alpha \mathbf{I}_M & \mathbf{0} \end{bmatrix} = \begin{bmatrix} \mathbf{R} & \mathbf{Q}^H \\ \mathbf{0} & ((\bar{\mathbf{Q}}^\perp)^{1, P})^H \end{bmatrix} \quad (51)$$

which yields only $((\bar{\mathbf{Q}}^\perp)^{1, P})^H$ as a by-product [3]. We note that since the $P \times P$ matrix $((\bar{\mathbf{Q}}^\perp)^{1, P})^H$ is larger than the $(P-M) \times P$ matrix $(\mathbf{Q}^\perp)^H$ in (4), obtained as a by-product of UT-based QR decomposition of \mathbf{A} , efficient UT-based regularized QR decomposition of \mathbf{A} exhibits higher complexity than UT-based QR decomposition of \mathbf{A} .

Finally, we note that since $\mathbf{Q} = \bar{\mathbf{Q}}^{1, P}$, applying the mapping \mathcal{M} to the regularized QR factors \mathbf{Q} and \mathbf{R} of \mathbf{A} according to (10)–(12) is equivalent to applying \mathcal{M} to the QR factors $\bar{\mathbf{Q}}$ and \mathbf{R} of $\bar{\mathbf{A}}$ to obtain $\tilde{\bar{\mathbf{Q}}}$ and $\tilde{\mathbf{R}}$ followed by extracting $\tilde{\mathbf{Q}} = \tilde{\bar{\mathbf{Q}}}^{1, P}$. With this insight, it is straightforward to verify that Theorem 9, formulated for QR decomposition of an LP matrix $\mathbf{A}(s)$, is valid for regularized QR decomposition of $\mathbf{A}(s)$ as well.

7.2. Application to MIMO-OFDM MMSE-Based Detectors

With the definition of regularized QR decomposition in the previous section, we recognize that MMSE-QR decomposition of $\mathbf{H}(s_n)$, defined in Section 3.2, is a special case of regularized QR decomposition of $\mathbf{H}(s_n)$ obtained by setting the regularization parameter α to $\sqrt{M_T}\sigma_w$. The modification of Algorithms I and II to the MMSE case is straightforward and simply amounts to replacing, in Step 2 of both algorithms, QR decomposition by MMSE-QR decomposition. The resulting algorithms are referred to as Algorithm I-MMSE and Algorithm II-MMSE, respectively.

In the following, we compare the complexity of Algorithm I-MMSE and Algorithm II-MMSE. By denoting the complexity associated with computing the MMSE-QR decomposition of an $M_R \times M_T$ matrix by $c_{\text{MMSE-QR}}^{M_R \times M_T}$, the overall complexity of Algorithms I-MMSE and II-MMSE is given by

$$C_{\text{I-MMSE}} = C_{\text{I}} + D \left(c_{\text{MMSE-QR}}^{M_R \times M_T} - c_{\text{QR}}^{M_R \times M_T} \right) \quad (52)$$

and

$$C_{\text{II-MMSE}} = C_{\text{II}} + B_{M_T} \left(c_{\text{MMSE-QR}}^{M_R \times M_T} - c_{\text{QR}}^{M_R \times M_T} \right) \quad (53)$$

respectively. Since $c_{\text{MMSE-QR}}^{M_R \times M_T} > c_{\text{QR}}^{M_R \times M_T}$, as explained in Section 7.1, (52) and (53) imply that $C_{\text{I-MMSE}} > C_{\text{I}}$ and $C_{\text{II-MMSE}} > C_{\text{II}}$, respectively. Thus, from (39), (40), (52), and (53), we get

$$\begin{aligned} \frac{C_{\text{II-MMSE}}}{C_{\text{II}}} &= \frac{(c_{\mathcal{M},\text{II}} + c_{\text{IP},\tilde{\mathbf{Q}}\tilde{\mathbf{R}},\text{II}} + c_{\mathcal{M}^{-1},\text{II}}) + B_{M_T} \left(c_{\text{IP},\mathbf{H}}^{1,M_T} + c_{\text{MMSE-QR}}^{M_R \times M_T} \right)}{(c_{\mathcal{M},\text{II}} + c_{\text{IP},\tilde{\mathbf{Q}}\tilde{\mathbf{R}},\text{II}} + c_{\mathcal{M}^{-1},\text{II}}) + B_{M_T} \left(c_{\text{IP},\mathbf{H}}^{1,M_T} + c_{\text{QR}}^{M_R \times M_T} \right)} \\ &< \frac{c_{\text{IP},\mathbf{H}}^{1,M_T} + c_{\text{MMSE-QR}}^{M_R \times M_T}}{c_{\text{IP},\mathbf{H}}^{1,M_T} + c_{\text{QR}}^{M_R \times M_T}} \\ &= \frac{C_{\text{I-MMSE}}}{C_{\text{I}}} \end{aligned} \quad (54)$$

where the inequality follows from the simple property

$$\alpha > \beta > 0, \gamma > 0 \implies \frac{\gamma + \alpha}{\gamma + \beta} < \frac{\alpha}{\beta}.$$

From (54) we can therefore conclude that

$$\frac{C_{\text{II-MMSE}}}{C_{\text{I-MMSE}}} < \frac{C_{\text{II}}}{C_{\text{I}}}$$

which implies, assuming $C_{\text{II}} < C_{\text{I}}$, that the relative savings of Algorithm II-MMSE over Algorithm I-MMSE are larger than the relative savings of Algorithm II over Algorithm I.

Finally, we briefly discuss the extension of Algorithm III to the MMSE case. As a starting point, we consider the straightforward approach of applying Algorithm III to the MMSE-augmented channel matrix $\tilde{\mathbf{H}}(s_n)$ in (9) to produce $\tilde{\mathbf{Q}}(s_n)$ and $\tilde{\mathbf{R}}(s_n)$ for all $n \in \mathcal{D}$. In the following, we denote by $\tilde{\tilde{\mathbf{Q}}}(s_n)$ and $\tilde{\tilde{\mathbf{R}}}(s_n)$ the matrices resulting from the application of the mapping \mathcal{M} to $(\tilde{\mathbf{Q}}(s_n), \tilde{\mathbf{R}}(s_n))$. We observe that the straightforward

approach under consideration is inefficient, since we are only interested in obtaining $\mathbf{Q}(s_n) = \bar{\mathbf{Q}}^{1,M_R}(s_n)$ and $\mathbf{R}(s_n)$ for all $n \in \mathcal{D}$. Consequently, we would like to avoid computing the last M_T rows of $\bar{\mathbf{Q}}(s_n)$ at as many tones as possible. Now, the reduction step (i.e., Step 4) in the k th iteration of Algorithm III requires knowledge of $\bar{\mathbf{Q}}_{1,k-1}(s_n)$ at the tones $n \in \mathcal{I}_k \setminus \mathcal{I}_{k-1}$ ($k = 2, 3, \dots, M_T$). Hence, at the tones $n \in \mathcal{I}_k \setminus \mathcal{I}_{k-1}$ we must compute all $M_R + M_T$ rows of $\bar{\mathbf{Q}}_{1,k-1}(s_n)$ anyway. In contrast, at the tones $n \in \mathcal{D} \setminus \mathcal{I}_{M_T}$ the last M_T rows of $\bar{\mathbf{Q}}(s_n)$ are not required. Therefore, at the tones $n \in \mathcal{D} \setminus \mathcal{I}_{M_T}$ we can restrict interpolation and inverse mapping to $\tilde{\mathbf{Q}}(s_n) = \tilde{\mathbf{Q}}^{1,M_R}(s_n)$ and $\tilde{\mathbf{R}}(s_n)$.

In the following, we partition $\tilde{\mathbf{q}}_k(s_n)$, the k th column of $\tilde{\mathbf{Q}}(s_n)$, as

$$\tilde{\mathbf{q}}_k(s_n) = \begin{bmatrix} \tilde{\mathbf{q}}_k(s_n) \\ \check{\mathbf{q}}_k(s_n) \end{bmatrix}, \quad k = 1, 2, \dots, M_T$$

with the $M_R \times 1$ vector $\tilde{\mathbf{q}}_k(s_n)$ and the $M_T \times 1$ vector $\check{\mathbf{q}}_k(s_n)$. With this notation, we can formulate the resulting algorithm as follows:

Algorithm III-MMSE

1. Set $k \leftarrow 1$.
2. Interpolate $\mathbf{H}_{k,M_T}(s)$ from $\mathcal{S}(\mathcal{E})$ to $\mathcal{S}(\mathcal{I}_k \setminus \mathcal{I}_{k-1})$.
3. For each $n \in \mathcal{I}_k \setminus \mathcal{I}_{k-1}$, construct $\bar{\mathbf{H}}_{k,M_T}(s_n)$ according to (9).
4. If $k = 1$, go to Step 6. Otherwise, for each $n \in \mathcal{I}_k \setminus \mathcal{I}_{k-1}$, apply $\mathcal{M}^{-1} : (\tilde{\mathbf{Q}}_{1,k-1}(s_n), \tilde{\mathbf{R}}^{1,k-1}(s_n)) \mapsto (\bar{\mathbf{Q}}_{1,k-1}(s_n), \mathbf{R}^{1,k-1}(s_n))$.
5. For each $n \in \mathcal{I}_k \setminus \mathcal{I}_{k-1}$, overwrite $\bar{\mathbf{H}}_{k,M_T}(s_n)$ by $\bar{\mathbf{H}}_{k,M_T}(s_n) - \bar{\mathbf{Q}}_{1,k-1}(s_n) \mathbf{R}_{k,M_T}^{1,k-1}(s_n)$.
6. For each $n \in \mathcal{I}_k \setminus \mathcal{I}_{k-1}$, perform QR decomposition on $\bar{\mathbf{H}}_{k,M_T}(s_n)$ to obtain $\bar{\mathbf{Q}}_{k,M_T}(s_n)$ and $\mathbf{R}_{k,M_T}^{k,M_T}(s_n)$, and, if $k > 1$, construct $\mathbf{R}^{k,M_T}(s_n) = [\mathbf{0} \quad \mathbf{R}_{k,M_T}^{k,M_T}(s_n)]$.
7. For each $n \in \mathcal{I}_k \setminus \mathcal{I}_{k-1}$, apply $\mathcal{M} : (\bar{\mathbf{Q}}_{k,M_T}(s_n), \mathbf{R}^{k,M_T}(s_n)) \mapsto (\tilde{\mathbf{Q}}_{k,M_T}(s_n), \tilde{\mathbf{R}}^{k,M_T}(s_n))$.^a
8. Interpolate $\tilde{\mathbf{q}}_k(s)$ and $\tilde{\mathbf{r}}_k^T(s)$ from $\mathcal{S}(\mathcal{I}_k)$ to $\mathcal{S}(\mathcal{D} \setminus \mathcal{I}_k)$.
9. If $k = M_T$, proceed to Step 11. Otherwise, interpolate $\check{\mathbf{q}}_k(s)$ from $\mathcal{S}(\mathcal{I}_k)$ to $\mathcal{S}(\mathcal{I}_{M_T} \setminus \mathcal{I}_k)$.
10. Set $k \leftarrow k + 1$ and go back to Step 2.
11. For each $n \in \mathcal{D} \setminus \mathcal{I}_{M_T}$, apply $\mathcal{M}^{-1} : (\tilde{\mathbf{Q}}(s_n), \tilde{\mathbf{R}}(s_n)) \mapsto (\mathbf{Q}(s_n), \mathbf{R}(s_n))$.

^aSince $\check{\mathbf{q}}_{M_T}(s_n)$ is not needed, its computation in the M_T th iteration can be skipped.

A detailed complexity analysis of Algorithm III-MMSE goes beyond the scope of this paper. We mention, however, the following important aspect of the comparison of Algorithm III-MMSE with Algorithms I-MMSE and II-MMSE. Step 2 of Algorithms I-MMSE and II-MMSE requires MMSE-QR decomposition, which is a special case of regularized QR decomposition, whereas Step 6 of Algorithm III-MMSE requires QR decomposition of an augmented matrix. As shown in Section 7.1, the algorithms for regularized QR decomposition and for QR decomposition of an augmented matrix have the same complexity under a GS-based

approach, but not under a UT-based approach. In the latter case, Algorithms I-MMSE and II-MMSE can perform efficient UT-based regularized QR decomposition according to the standard form (51), whereas Algorithm III-MMSE must perform UT-based QR decomposition of an augmented matrix according to the standard form (49), which results in higher complexity. This aspect does not occur in the comparison of Algorithm III with Algorithms I and II and will be further examined numerically in Section 9.2.

8. Efficient Interpolation

Throughout this section, we consider interpolation of a generic LP $a(s) \sim (V_1, V_2)$ of maximum degree $V = V_1 + V_2$ from \mathcal{B} to \mathcal{T} , where $|\mathcal{B}| = B$ and $|\mathcal{T}| = T$. We note that in the context of interpolation in MIMO-OFDM systems, relevant for the algorithms presented in this paper, all base points and all target points correspond to OFDM tones. Therefore, in the following we assume that \mathcal{B} and \mathcal{T} satisfy the condition

$$\mathcal{B} \cup \mathcal{T} \subseteq \{s_0, s_1, \dots, s_{N-1}\}. \quad (55)$$

The complexity analysis in Section 6 showed that interpolation-based QR decomposition algorithms yield savings over the brute-force approach only if c_{IP} is sufficiently small. Straightforward interpolation of $a(s)$, which corresponds to direct evaluation of (8), is performed by carrying out the multiplication of the $T \times B$ interpolation matrix \mathbf{TB}^\dagger by the $B \times 1$ vector $\mathbf{a}_{\mathcal{B}}$. The corresponding complexity is given by TB , which results in $c_{\text{IP}} = B$ full multiplications per target point. In the context of interpolation-based QR decomposition, this complexity may be too high to get savings over the brute-force approach in Algorithms I or I-MMSE, since exact interpolation of $\tilde{\mathbf{q}}_k(s) \sim (kL, kL)$ and $\tilde{\mathbf{r}}_k^T(s) \sim (kL, kL)$ requires $B \geq 2kL + 1$ ($k = 1, 2, \dots, M_T$), with the worst case being $B \geq 2M_T L + 1$. In this section, we present interpolation methods characterized by significantly smaller values of c_{IP} . As demonstrated by the numerical results in Section 9, this can then lead to significant savings of the interpolation-based approaches for QR decomposition over the brute-force approach.

8.1. Interpolation with Dedicated Multipliers

As already noted, the interpolation matrix \mathbf{TB}^\dagger is a function of \mathcal{B} , \mathcal{T} , V_1 and V_2 , but not of the realization of the LP $a(s)$ to be interpolated. Hence, as long as \mathcal{B} , \mathcal{T} , V_1 and V_2 do not change, multiple LPs can be interpolated using the same interpolation matrix \mathbf{TB}^\dagger , which can be computed off-line. This observation leads to the first strategy for efficient interpolation, which consists of carrying out the matrix-vector product $(\mathbf{TB}^\dagger)\mathbf{a}_{\mathcal{B}}$ in (8) through TB constant multiplications, where the entries of \mathbf{TB}^\dagger are constant and the entries of $\mathbf{a}_{\mathcal{B}}$ are variable.

In the context of VLSI implementation, full multiplications and constant multiplications differ significantly. Whereas a full multiplication must be performed by a *full multiplier* which processes two variable

operands, in a constant multiplication, the fact that one of the operands, and more specifically its binary representation, is known a priori, can be exploited to perform binary logic simplifications that result in a drastically simpler circuit [10]. The resulting multiplier, called a *dedicated multiplier* in the following, consumes only a fraction of the silicon area (down to 1/9, as reported in [7] for complex-valued dedicated multipliers) required by a full multiplier, and exhibits the same processing delay. Furthermore, we mention that it is possible to obtain further area savings, again without affecting the processing delay, by merging K dedicated multipliers into a single block multiplier that jointly performs the K multiplications, according to a technique known as *partial product sharing* [11], which essentially exploits common bit patterns in the binary representations of the K coefficients to obtain circuit simplifications. For simplicity of exposition, in the sequel we do not consider partial product sharing.

In the remainder of the paper, $\chi_{\mathbb{C}}$ and $\chi_{\mathbb{R}}$ denote the complexity associated with a constant multiplication of a complex-valued variable operand by a complex-valued and by a real-valued constant coefficient, respectively. Since \mathbf{TB}^\dagger is real-valued for $V_1 = V_2$ and complex-valued otherwise, interpolation through constant multiplications with dedicated multipliers has a complexity per target point of

$$c_{\text{IP}} = \begin{cases} \chi_{\mathbb{R}}B, & V_1 = V_2 \\ \chi_{\mathbb{C}}B, & V_1 \neq V_2. \end{cases}$$

By leaving a cautionary implementation margin from the best-effort value of 1/9 reported in [7], we assume that $\chi_{\mathbb{C}} = 1/4$ in the remainder of the paper. Since the multiplication of two complex-valued numbers requires (assuming straightforward implementation) four real-valued multiplications, whereas multiplying a real-valued number by a complex-valued number requires only two real-valued multiplications, we henceforth assume that $\chi_{\mathbb{R}} = \chi_{\mathbb{C}}/2$, which leads to $\chi_{\mathbb{R}} = 1/8$.

8.2. Equidistant Base Points

In the following, we say that the points in a set $\{u_0, u_1, \dots, u_{K-1}\} \subset \mathcal{U}$ are *equidistant on \mathcal{U}* if $u_k = u_0 e^{j2\pi k/K}$ for $k = 1, 2, \dots, K-1$. So far, we discussed interpolation of $a(s) \sim (V_1, V_2)$ for generic sets \mathcal{B} and \mathcal{T} . In the remainder of Section 8 we will, however, focus on the following special case. Given integers $B, R > 1$, we consider the set of B base points $\mathcal{B} = \{b_k = e^{j2\pi k/B} : k = 0, 1, \dots, B-1\}$ and the set of $T = (R-1)B$ target points $\mathcal{T} = \{t_{(R-1)k+r-1} = b_k e^{j2\pi r/(RB)} : k = 0, 1, \dots, B-1, r = 1, 2, \dots, R-1\}$. We note that both the B points in \mathcal{B} and the RB points in $\mathcal{B} \cup \mathcal{T} = \{e^{j2\pi l/(RB)} : l = 0, 1, \dots, RB-1\}$ are equidistant on \mathcal{U} . Hence, interpolation of $a(s)$ from \mathcal{B} to \mathcal{T} essentially amounts to an R -fold increase in the sampling rate of $a(s)$ on \mathcal{U} , and will therefore be termed *upsampling of $a(s)$ from B equidistant base points by a factor of R* in the remainder of the paper. The corresponding base point matrix \mathbf{B} and target point matrix \mathbf{T} are constructed according to (6) and (7), respectively. We note that for $B \geq V+1$, \mathbf{B} satisfies $\mathbf{B}^H \mathbf{B} = B \mathbf{I}_B$ and hence $\mathbf{B}^\dagger = (1/B) \mathbf{B}^H$.

We recall that the number of OFDM tones N is typically a power of two. Therefore, in order to have RB equidistant points on \mathcal{U} while satisfying the condition (55), in the following we constrain both B and R to be powers of two. Finally, in order to satisfy the condition $B \geq V + 1$ mandated by the requirement of exact interpolation, we set $B = 2^{\lceil \log(V+1) \rceil}$.

8.3. Interpolation by Fast Fourier Transform

In the context of upsampling from B equidistant base points by a factor of R , it is straightforward to verify that the $B \times (V + 1)$ matrix \mathbf{B} is given by

$$\mathbf{B} = [(\mathbf{W}_B)_{B-V_1+1, B} \quad (\mathbf{W}_B)_{1, V_2+1}] \quad (56)$$

and that the $(R - 1)B \times (V + 1)$ matrix \mathbf{T} is obtained by removing the rows with indices in $\mathcal{R} \triangleq \{1, R + 1, \dots, (B - 1)R + 1\}$ from the $RB \times (V + 1)$ matrix

$$\bar{\mathbf{T}} \triangleq [(\mathbf{W}_{RB})_{RB-V_1+1, RB} \quad (\mathbf{W}_{RB})_{1, V_2+1}]. \quad (57)$$

As done in Section 2.3, we consider the vectors $\mathbf{a} = [a_{-V_1} \ a_{-V_1+1} \ \dots \ a_{V_2}]^T$, $\mathbf{a}_{\mathcal{B}} = \mathbf{B}\mathbf{a}$, and $\mathbf{a}_{\mathcal{T}} = \mathbf{T}\mathbf{a}$. By defining the B -dimensional vector $\mathbf{a}^{(B)} \triangleq [a_0 \ a_1 \ \dots \ a_{V_2} \ 0 \ \dots \ 0 \ a_{-V_1} \ a_{-V_1+1} \ \dots \ a_{-1}]^T$, which contains $B - (V + 1)$ zeros between the entries a_{V_2} and a_{-V_1} , and by taking (56) into account, we can write $\mathbf{a}_{\mathcal{B}} = \mathbf{B}\mathbf{a} = \mathbf{W}_B\mathbf{a}^{(B)}$, from which follows that $\mathbf{a}^{(B)} = \mathbf{W}_B^{-1}\mathbf{a}_{\mathcal{B}}$. Next, we insert $(R - 1)B$ zeros into $\mathbf{a}^{(B)}$ after the entry a_{V_2} to obtain the RB -dimensional vector $\mathbf{a}^{(RB)} \triangleq [a_0 \ a_1 \ \dots \ a_{V_2} \ 0 \ \dots \ 0 \ a_{-V_1} \ a_{-V_1+1} \ \dots \ a_{-1}]^T$. Further, we define $\mathbf{a}_{\mathcal{B} \cup \mathcal{T}} \triangleq [a(e^{j0}) \ a(e^{j2\pi/RB}) \ \dots \ a(e^{j2\pi(RB-1)/RB})]^T = \bar{\mathbf{T}}\mathbf{a}$ to be the vector containing the samples of $a(s)$ at the points in $\mathcal{B} \cup \mathcal{T}$. We note that using (57) we can write

$$\bar{\mathbf{T}}\mathbf{a} = \mathbf{W}_{RB}\mathbf{a}^{(RB)}. \quad (58)$$

Next, we observe that by removing the rows with indices in \mathcal{R} from both sides of the equality $\mathbf{a}_{\mathcal{B} \cup \mathcal{T}} = \bar{\mathbf{T}}\mathbf{a}$ we obtain the equality $\mathbf{a}_{\mathcal{T}} = \mathbf{T}\mathbf{a}$. The latter observation, combined with (58), implies that $\mathbf{a}_{\mathcal{T}}$ can be obtained by removing the rows with indices in \mathcal{R} from the vector $\mathbf{W}_{RB}\mathbf{a}^{(RB)}$. Finally, we note that since B and RB are powers of two, left-multiplication by \mathbf{W}_B^{-1} and \mathbf{W}_{RB} can be computed through a B -point radix-2 inverse FFT (IFFT) and an RB -point radix-2 FFT, respectively [2]. We can therefore conclude that FFT-based interpolation of $a(s)$ from \mathcal{B} to \mathcal{T} can be carried out as follows:

1. Compute the B -point radix-2 IFFT $\mathbf{a}^{(B)} = \mathbf{W}_B^{-1}\mathbf{a}_{\mathcal{B}}$.
2. Construct $\mathbf{a}^{(RB)}$ from $\mathbf{a}^{(B)}$ by inserting $(R - 1)B$ zeros after the entry a_{V_2} in $\mathbf{a}^{(B)}$.
3. Compute the RB -point radix-2 FFT $\mathbf{a}_{\mathcal{B} \cup \mathcal{T}} = \mathbf{W}_{RB}\mathbf{a}^{(RB)}$.
4. Extract $\mathbf{a}_{\mathcal{T}}$ from $\mathbf{a}_{\mathcal{B} \cup \mathcal{T}}$ by removing the entries of $\mathbf{a}_{\mathcal{B} \cup \mathcal{T}}$ with indices in \mathcal{R} .

Now, we note that if generic radix-2 IFFT and FFT algorithms are used in Steps 1 and 3, respectively, the approach described above does not exploit the structure of the problem at hand and is inefficient in the following three aspects. First, neither the IFFT in Step 1 nor the FFT in Step 3 take into account that $B - (V + 1)$ entries of $\mathbf{a}^{(B)}$ (and also, by construction, of $\mathbf{a}^{(RB)}$) are zero. As this inefficiency does not arise in the case $B = V + 1$ and has only marginal impact on interpolation complexity otherwise, we will not consider it further. Second, the FFT in Step 3 ignores the fact that $\mathbf{a}^{(RB)}$ contains the $(R - 1)B$ zeros that were inserted in Step 2. Third, the values of $a(s)$ at the base points, which are already known prior to interpolation, are unnecessarily computed by the FFT in Step 3 and then discarded in Step 4. In the following, we present a modified FFT algorithm, tailored to the problem at hand, which eliminates the latter two inefficiencies and leads to a significantly lower interpolation complexity than the generic FFT-based interpolation method described above.

From now on, in order to simplify the notation, we assume that $N = RB$. Thus, with $s_n = e^{j2\pi n/N}$, $n = 0, 1, \dots, N - 1$, the base points and the target points are given by $b_k = s_{Rk}$ and $t_{(R-1)k+r-1} = s_{Rk+r}$ ($k = 0, 1, \dots, B - 1$, $r = 1, 2, \dots, R - 1$), respectively. The derivation presented in the following will be illustrated through an example obtained by setting $B = R = 4$ and $V_1 = V_2 + 1 = 2$, but is valid in general for the case where V_1 and V_2 satisfy the inequalities $0 \leq V_1 \leq B/2$ and $0 \leq V_2 \leq B/2 - 1$, respectively. We note that these two inequalities, combined with $B = 2^{\lceil \log(V_1 + V_2 + 1) \rceil}$, are satisfied in the case $V_1 = V_2$. Hence, the following derivation covers the case of interpolation of the entries of $\tilde{\mathbf{Q}}(s) \sim (M_T L, M_T L)$ and $\tilde{\mathbf{R}}(s) \sim (M_T L, M_T L)$, as required in Algorithms II, III, II-MMSE and III-MMSE.

The proposed modified FFT is based on a decimation-in-time radix-2 N -point FFT, consisting of a scrambling stage followed by $\log N$ computation stages [2], each containing $N/2$ radix-2 butterflies described by the signal flow graph (SFG) in Fig. 1a. The twiddle factors used in the FFT butterflies are powers of $\omega_N \triangleq e^{-j2\pi/N}$.

The SFG of the unmodified N -point FFT is shown in Fig. 1b. We observe that the scrambling stage at the beginning of the FFT (not depicted in Fig. 1b) causes the nonzero entries $a_{-V_1}, a_{-V_1+1}, \dots, a_{V_2}$ of $\mathbf{a}^{(RB)}$ to be scattered rather than to appear in blocks as is the case in $\mathbf{a}^{(RB)}$. The main idea of the proposed approach is to prune all SFG branches that involve multiplications and additions with operands equal to zero, as done in [15],⁵ and all SFG branches that lead to the computation of the already known values of $a(s)$ at the base points. The SFG of the resulting pruned FFT is shown in Fig. 2a.

Further complexity reductions can be obtained as follows. We observe that in the pruned FFT, the SFG branches departing from a_0, a_1, \dots, a_{V_2} contain no arithmetic operations in the first $\log R$ computation stages. In contrast, the SFG branches departing from $a_{-V_1}, a_{-V_1+1}, \dots, a_{-1}$ contain multiplications by twiddle factors in each of the first $\log R$ computation stages. These multiplications can however be shifted

⁵The SFG pruning approach proposed in [15] applies to the case $V_1 = 0$ only.

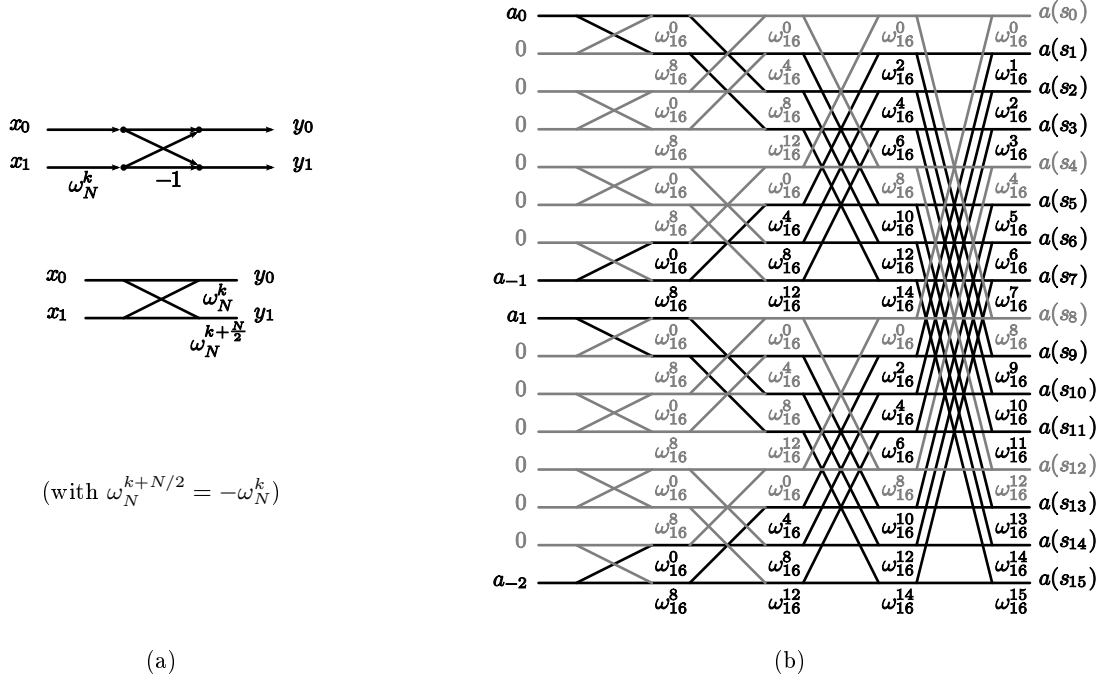


Figure 1: (a) SFG of a radix-2 butterfly (top) with twiddle factor ω_N^k , and alternative, equivalent representation (bottom) needed for compact illustration in FFT SFGs. (b) SFG of the full N -point radix-2 decimation-in-time FFT, without the scrambling stage. $N = RB$, $B = R = 4$, $V_1 = V_2 + 1 = 2$. SFG branches depicted in grey will be pruned.

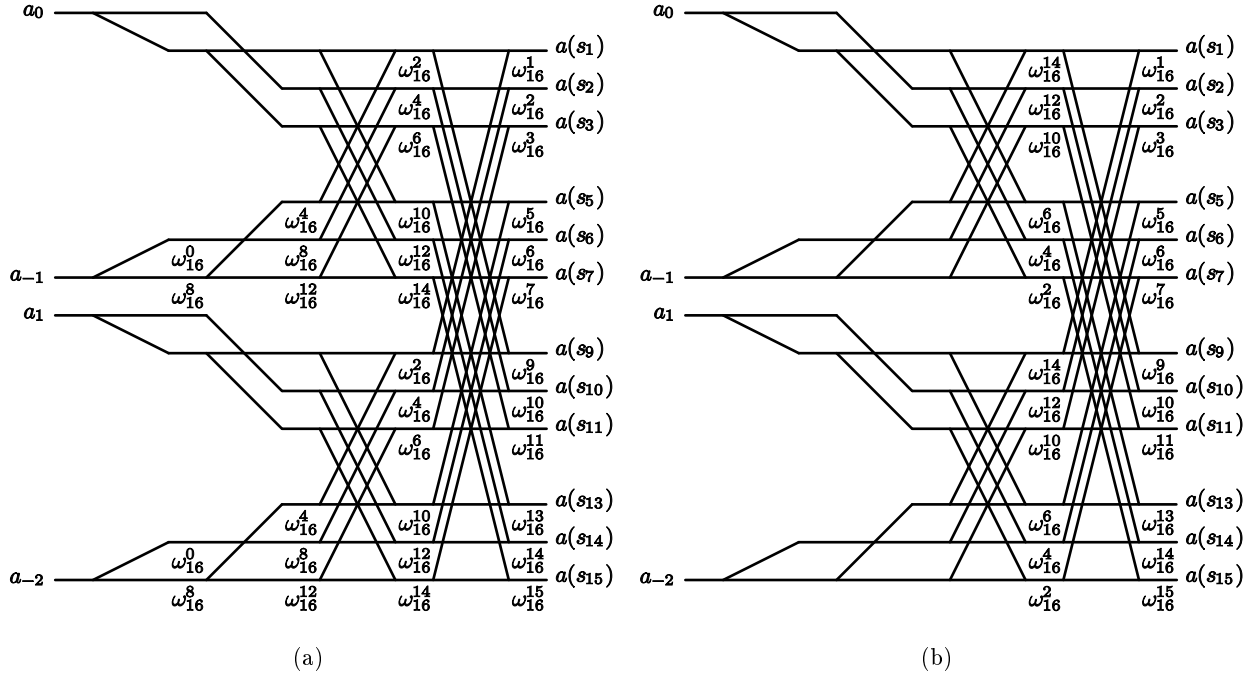


Figure 2: SFG of the pruned N -point FFT, without the scrambling stage, before (a) and after (b) shifting all multiplications from the first $\log R$ stages into stage $1 + \log R$. $N = RB$, $B = R = 4$, $V_1 = V_2 + 1 = 2$.

into computation stage $1 + \log R$ through basic SFG transformations. The result is the modified FFT illustrated in Fig. 2b, for which the first $\log R$ computation stages do not contain any arithmetic operations and therefore have zero complexity, whereas the last $\log B$ computation stages contain $(R-1)B/2$ butterflies each. Thus, since each radix-2 butterfly entails one full multiplication,⁶ the total complexity of FFT-based interpolation of $\mathbf{a}(s)$ from \mathcal{B} to \mathcal{T} is determined by the $(B/2)\log B$ full multiplications required by the B -point radix-2 IFFT $\mathbf{a}^{(B)} = \mathbf{W}_B^{-1}\mathbf{a}_B$ and the $(R-1)(B/2)\log B$ full multiplications required in the last $\log B$ computation stages of the proposed modified RB -point FFT, which computes \mathbf{a}_T from $\mathbf{a}^{(RB)}$. The corresponding interpolation complexity per target point is therefore given by

$$c_{\text{IP,FFT}} \triangleq \frac{\left(\frac{B}{2}\log B\right) + \left((R-1)\frac{B}{2}\log B\right)}{(R-1)B} = \frac{1}{2}\frac{R}{R-1}\log B. \quad (59)$$

We mention that a modified RB -point FFT can be derived, analogously to above, also in the case $V_1 = 0$ (for which $V = V_2$ and $B = 2^{\lceil \log(V_2+1) \rceil}$), relevant for interpolation of $\mathbf{H}(s) \sim (0, L)$ in Algorithms I–III and I-MMSE through III-MMSE. The corresponding interpolation complexity per target point is again given by (59).

Finally, we note that in MIMO-OFDM transceivers the FFT processor that performs N -point IFFT/FFT for OFDM modulation/demodulation can be reused with slight modifications to carry out the B -point IFFT and the proposed modified RB -point FFT that are needed for interpolation. Such a resource sharing approach reduces the silicon area associated with interpolation and hence further reduces $c_{\text{IP,FFT}}$. The resulting savings will, for the sake of generality of exposition, not be taken into account in the following.

8.4. Interpolation by FIR Filtering

We consider upsampling of $a(s)$ from B equidistant base points by a factor of R , as defined in Section 8.2. The derivations in this section are valid for arbitrary integers $B, R > 1$, and hence not specific to the case where B and R are powers of two.

Proposition 11. *In the context of upsampling from B equidistant base points by a factor of R , the $B(R-1) \times B$ interpolation matrix \mathbf{TB}^\dagger satisfies the following properties:*

1. *There exists an $(R-1) \times B$ matrix \mathbf{F}_0 such that \mathbf{TB}^\dagger can be written as*

$$\mathbf{TB}^\dagger = \begin{bmatrix} \mathbf{F}_0 \mathbf{C}_B \\ \mathbf{F}_0 \mathbf{C}_B^2 \\ \vdots \\ \mathbf{F}_0 \mathbf{C}_B^B \end{bmatrix} \quad (60)$$

⁶We assume that the FFT processor does not use any dedicated multipliers.

with the $B \times B$ circulant matrix

$$\mathbf{C}_B \triangleq \begin{bmatrix} \mathbf{0} & \mathbf{I}_{B-1} \\ 1 & \mathbf{0} \end{bmatrix}.$$

2. The matrix \mathbf{F}_0 , as implicitly defined in (60), satisfies

$$[\mathbf{F}_0]_{r,k+1} = [\mathbf{F}_0]_{R-r,B-k}^*, \quad r = 1, 2, \dots, R-1, \quad k = 0, 1, \dots, B-1.$$

Proof. Since $\mathbf{B}^\dagger = (1/B)\mathbf{B}^H$, the entries of \mathbf{TB}^\dagger are given by

$$[\mathbf{TB}^\dagger]_{k(R-1)+r,k'+1} = \frac{1}{B} \sum_{v=-V_1}^{V_2} e^{-j2\pi v \frac{R(k-k')+r}{RB}} \quad (61)$$

for $k, k' = 0, 1, \dots, B-1$ and $r = 1, 2, \dots, R-1$. The two properties are now established as follows:

1. The RHS of (61) remains unchanged upon replacing k and k' by $(k+1) \bmod B$ and $(k'+1) \bmod B$, respectively. Hence, for a given $r \in \{1, 2, \dots, R-1\}$, the $B \times B$ matrix obtained by stacking the rows indexed by $r, (R-1)+r, \dots, (B-1)(R-1)+r$ (in this order) of \mathbf{TB}^\dagger is circulant. By taking \mathbf{F}_0 to consist of the last $R-1$ rows of \mathbf{TB}^\dagger , and using $\mathbf{C}_B^B = \mathbf{I}_B$, along with the fact that for $b \in \mathbb{Z}$, the multiplication $\mathbf{F}_0 \mathbf{C}_B^b$ corresponds to circularly shifting the columns of \mathbf{F}_0 to the right by $b \bmod B$ positions, we obtain (60).
2. The entries of \mathbf{F}_0 are obtained by setting $k = B-1$ in (61) and are given by

$$[\mathbf{F}_0]_{r,k'+1} = \frac{1}{B} \sum_{v=-V_1}^{V_2} e^{-j2\pi v \frac{r-R(k'+1)}{RB}}, \quad r = 1, 2, \dots, R-1, \quad k' = 0, 1, \dots, B-1.$$

Hence, for $r = 1, 2, \dots, R-1$ and $k' = 0, 1, \dots, B-1$, we obtain

$$\begin{aligned} [\mathbf{F}_0]_{R-r,B-k'}^* &= \frac{1}{B} \sum_{v=-V_1}^{V_2} e^{j2\pi v \frac{R-r-R(B-k')}{RB}} \\ &= \frac{1}{B} \sum_{v=-V_1}^{V_2} e^{-j2\pi v \frac{r-R(k'+1)}{RB}} \\ &= [\mathbf{F}_0]_{r,k'+1}. \end{aligned}$$

□

We note that Property 1 in Proposition 11 implies that the matrix-vector multiplication $(\mathbf{TB}^\dagger)\mathbf{a}_B$ in (8) can be carried out through the application of $R-1$ FIR filters. Specifically, for $r = 1, 2, \dots, R-1$, the entries $r, r+R, \dots, r+(B-1)R$ of \mathbf{a}_T can be obtained by computing the circular convolution of \mathbf{a}_B with the impulse response of length B contained in the r th row of \mathbf{F}_0 . In the remainder of the paper, we will say that the $R-1$ FIR filters are *defined* by \mathbf{F}_0 . By allocating B dedicated multipliers per FIR filter (one

per impulse response tap), we would need a total of $(R - 1)B$ dedicated multipliers. We will next see that the complex-conjugate symmetry in the rows of \mathbf{F}_0 , formulated as Property 2 in Proposition 11, allows to reduce the number of dedicated multipliers and the interpolation complexity by a factor of two.

In the following, we assume that the multiplications of a variable complex-valued operand by a constant $\gamma \in \mathbb{C}$ and by its complex conjugate γ^* can be carried out using the same dedicated multiplier, and that the resulting complexity is comparable to the complexity of multiplication by γ alone. This is justified as the multiplication by γ^* , compared to the multiplication by γ , involves the same four underlying real-valued multiplications and only requires two additional sign flips, which have significantly smaller complexity than the real-valued multiplications. Thus, we can perform multiplication by the coefficients $[\mathbf{F}_0]_{r,k+1}$ and $[\mathbf{F}_0]_{R-r,B-k} = [\mathbf{F}_0]_{r,k+1}^*$ through a single dedicated multiplier ($r = 1, 2, \dots, R/2$, $k = 0, 1, \dots, B/2 - 1$). This resource sharing approach leads to

$$c_{\text{IP}} = \begin{cases} \frac{X_{\mathbb{R}}}{2}B, & V_1 = V_2 \\ \frac{X_{\mathbb{C}}}{2}B, & V_1 \neq V_2. \end{cases} \quad (62)$$

So far, we assumed that $a(s)$ is interpolated from the $B = 2^{\lceil \log(V+1) \rceil}$ base points in \mathcal{B} , resulting in c_{IP} according to (62). We will next show that the interpolation complexity can be further reduced by using a smaller number of base points $B' < B$. Interpolation will be exact as long as the condition $B' \geq V + 1$ is satisfied.

As done above, we assume knowledge of the B samples $a(s)$, $s \in \mathcal{B}$. In the following, however, we require that for a given target point t_r , the sample $a(t_r)$ is obtained by interpolation from only B' base points, picked from the B elements of \mathcal{B} as a function of t_r . For simplicity of exposition, we assume that B' is even, and for every $t_r \in \mathcal{T}$ we choose the B' elements of \mathcal{B} that are located closest to t_r on \mathcal{U} . We will next show that the resulting interpolation of $a(s)$ from \mathcal{B} to \mathcal{T} can be performed through FIR filtering.

In the following, we define B disjoint subsets \mathcal{T}_k of \mathcal{T} (satisfying $\mathcal{T}_0 \cup \mathcal{T}_1 \cup \dots \cup \mathcal{T}_{B-1} = \mathcal{T}$) and consider the corresponding subsets \mathcal{B}_k of \mathcal{B} , defined such that for all points in \mathcal{T}_k , the B' closest base points are given by the elements of \mathcal{B}_k ($k = 0, 1, \dots, B - 1$). We next show that the interpolation matrix corresponding to interpolation of $a(s)$ from \mathcal{B}_k to \mathcal{T}_k is independent of k . To this end, we first consider the set of target points $\mathcal{T}_0 \triangleq \{t_{(B-1)(R-1)+r-1} : r = 1, 2, \dots, R-1\}$, containing the $R-1$ target points located on \mathcal{U} between the base points b_{B-1} and b_0 . The subset of \mathcal{B} containing the B' points that are closest to every point in \mathcal{T}_0 is given by $\mathcal{B}_0 \triangleq \{b_0, b_1, \dots, b_{B'/2}, b_{B-B'/2}, b_{B-B'/2+1}, \dots, b_{B-1}\}$. Interpolation of $a(s)$ from \mathcal{B}_0 to \mathcal{T}_0 involves the base point matrix \mathbf{B}_0 , the target point matrix \mathbf{T}_0 , and the interpolation matrix $\mathbf{T}_0 \mathbf{B}_0^\dagger$, constructed as described in Section 2.3. Next, for $k = 1, 2, \dots, B-1$, we denote by \mathcal{B}_k and \mathcal{T}_k the sets obtained by multiplying all elements of \mathcal{B}_0 and \mathcal{T}_0 , respectively, by $e^{j2\pi k/B}$. We note that \mathcal{T}_k contains the $R-1$ target points located on \mathcal{U} between the base points b_{k-1} and b_k , and that \mathcal{B}_k is the subset of \mathcal{B} containing the B' points that are closest to every point in \mathcal{T}_k . With the unitary matrix $\mathbf{S}_k \triangleq \text{diag}((e^{j2\pi k/B})^{V_1}, (e^{j2\pi k/B})^{V_1-1}, \dots, (e^{j2\pi k/B})^{-V_2})$, interpolation

of $a(s)$ from \mathcal{B}_k to \mathcal{T}_k involves the base point matrix $\mathbf{B}_k = \mathbf{B}_0 \mathbf{S}_k$, with pseudoinverse $\mathbf{B}_k^\dagger = \mathbf{S}_k^{-1} \mathbf{B}_0^\dagger$, the target point matrix $\mathbf{T}_k = \mathbf{T}_0 \mathbf{S}_k$, and the interpolation matrix $\mathbf{T}_k \mathbf{B}_k^\dagger = \mathbf{T}_0 \mathbf{S}_k \mathbf{S}_k^{-1} \mathbf{B}_0^\dagger = \mathbf{T}_0 \mathbf{B}_0^\dagger$ ($k = 1, 2, \dots, B-1$). Hence, the interpolation matrix is independent of k and is the same as in the interpolation of $a(s)$ from \mathcal{B}_0 to \mathcal{T}_0 .

Now, interpolation of $a(s)$ from \mathcal{B} to \mathcal{T} , with the constraint that the sample of $a(s)$ at every target point is computed only from the samples of $a(s)$ at the B' closest base points, amounts to performing interpolation of $a(s)$ from \mathcal{B}_k to \mathcal{T}_k for all $k = 0, 1, \dots, B-1$, and can be written in a single equation as $\mathbf{a}_{\mathcal{T}} = \mathbf{F} \mathbf{a}_{\mathcal{B}}$. Here, the $(R-1)B \times B$ interpolation matrix \mathbf{F} is equal to the RHS of (60), with the $(R-1) \times B$ matrix

$$\mathbf{F}_0 = [(\mathbf{T}_0 \mathbf{B}_0^\dagger)_{1, B'/2} \quad \mathbf{0} \quad (\mathbf{T}_0 \mathbf{B}_0^\dagger)_{B-B'/2+1, B}] \quad (63)$$

which contains an all-zero submatrix of dimension $(R-1) \times (B-B')$. Hence, \mathbf{F} satisfies Property 1 of Proposition 11, with \mathbf{F}_0 given by (63). In addition, we state without proof that \mathbf{F}_0 in (63) satisfies Property 2 of Proposition 11. We can therefore conclude that interpolation from the closest B' base points maintains the structural properties of interpolation from all B base points and, as above, can be performed by FIR filtering using $R-1$ filters with dedicated multipliers that exploit the conjugate symmetry in the rows of \mathbf{F}_0 . Since the rows of \mathbf{F}_0 in (63) contain $B-B'$ zeros, the $R-1$ impulse responses now have length B' , and we obtain

$$c_{\text{IP}} = \begin{cases} \frac{\chi_{\text{E}}}{2} B', & V_1 = V_2 \\ \frac{\chi_{\text{C}}}{2} B', & V_1 \neq V_2. \end{cases} \quad (64)$$

8.5. Inexact Interpolation

The interpolation complexity (64) of the approach described in Section 8.4 can be further reduced by choosing B' to be smaller than $V+1$. This comes, however, at the cost of a systematic interpolation error and consequently leads to a trade-off between interpolation complexity and interpolation accuracy. In the context of MIMO-OFDM detectors, it is demonstrated in Section 9.1 that the performance degradation resulting from this systematic interpolation error is often negligible. In the following, we propose an ad-hoc method for inexact interpolation. The basic idea consists of introducing an interpolation error metric and formulating a corresponding optimization problem, which yields the matrix \mathbf{F}_0 that defines the FIR filters for inexact interpolation.

For simplicity of exposition, we restrict our discussion to inexact interpolation of $\tilde{\mathbf{Q}}(s) \sim (M_T L, M_T L)$ and $\tilde{\mathbf{R}}(s) \sim (M_T L, M_T L)$ with $V_1 = V_2 = M_T L$, as required in Step 4 of Algorithm II. For random-valued MIMO channel taps $\mathbf{H}_0, \mathbf{H}_1, \dots, \mathbf{H}_L$, we propose to quantify the interpolation error according to

$$e(\mathbf{F}_0) \triangleq \mathbb{E} \left[\sum_{n \in \mathcal{D} \setminus \mathcal{I}_{M_T}} \|\mathbf{Q}^H(s_n) \mathbf{H}(s_n) - \mathbf{R}(s_n)\|_2^2 \right] \quad (65)$$

where the expectation is taken over $\mathbf{H}_0, \mathbf{H}_1, \dots, \mathbf{H}_L$, and where the dependence of the RHS of (65) on \mathbf{F}_0 is implicit through the fact that within Algorithm II, the computation of $\mathbf{Q}(s_n)$ and $\mathbf{R}(s_n)$ at the tones $n \in \mathcal{D} \setminus \mathcal{I}_{M_T}$ involves interpolation through the FIR filters defined by \mathbf{F}_0 . We mention that the metric $e(\mathbf{F}_0)$ in (65) is relevant for MIMO-OFDM sphere decoding, and that minimization of $e(\mathbf{F}_0)$ does not necessarily lead to optimal detection performance. Other applications involving QR decomposition of polynomial matrices may require alternative error metrics.

For upsampling from B equidistant base points by a factor of R , under the condition $V_1 = V_2$, the matrix \mathbf{F}_0 in (63) is a function of N, R, B, B' , and V_1 . Now, we have that N is a fixed system parameter and $B = 2^{\lceil \log(2M_T L + 1) \rceil}$. Moreover, R is determined by N, B , and \mathcal{D} , since R is either given by $R = N/B$ in the case $|\mathcal{D}| = N$ or is a function of B and \mathcal{D} in the case $|\mathcal{D}| < N$. Finally, under a fixed complexity budget (i.e., a given value for c_{IP}), B' is constrained by (64). Now, $\tilde{\mathbf{Q}}(s), \tilde{\mathbf{R}}(s) \sim (M_T L, M_T L)$ determines $V_1 = M_T L$, but we propose, instead, to consider V_1 as a variable parameter, so that $\mathbf{F}_0 = \mathbf{F}_0(V_1)$. The interpolation error is then minimized by first determining

$$V_1' \triangleq \arg \min_{V_1 \in \{1, 2, \dots, M_T L\}} e(\mathbf{F}_0(V_1))$$

numerically, and then performing interpolation through the FIR filters defined by $\mathbf{F}_0(V_1')$.

9. Numerical Results

The results presented so far do not depend on a specific QR decomposition method. For the numerical complexity comparisons presented in this section, we will get more specific and assume UT-based QR decomposition performed through Givens rotations and coordinate rotation digital computer (CORDIC) operations [18, 19], which is the method of choice in VLSI implementations [3, 12]. For $\mathbf{A} \in \mathbb{C}^{P \times M}$ with $P \geq M$, it was shown in [3] that the complexity of UT-based QR decomposition of \mathbf{A} according to the standard form (4), as required in Algorithms I–III, is given by

$$c_{\text{QR}}^{P \times M} \triangleq \frac{3}{2}(P^2 M + P M^2) - M^3 - \frac{1}{2}(P^2 - P + M^2 + M)$$

and that the complexity of efficient UT-based regularized QR decomposition of \mathbf{A} according to the standard form (51), as required in Algorithms I-MMSE and II-MMSE, is given⁷ by

$$c_{\text{MMSE-QR}}^{P \times M} \triangleq \frac{3}{2}(P^2 M + P M^2) - \frac{1}{2}P^2 + \frac{1}{2}P. \quad (66)$$

The results in [3] carry over, in a straightforward fashion, to UT-based QR decomposition of the augmented matrix $[\mathbf{A}^T \quad \alpha \mathbf{I}_M]^T$ according to the standard form (49), as required in Algorithm III-MMSE, to yield

$$c_{\text{QR,III-MMSE}}^{P \times M} \triangleq c_{\text{MMSE-QR}}^{P \times M} + \frac{3}{2}P M^2 + \frac{1}{2}P M.$$

⁷In [3], the last term on the RHS of (66) was erroneously specified as $-(1/2)P$.

9.1. Efficient Interpolation and Performance Degradation

We start by quantifying the trade-off between interpolation complexity and detection performance, described in Section 8.5. Specifically, we evaluate the loss in detection performance as we gradually reduce B' , and hence also c_{IP} , in the interpolation of $\tilde{\mathbf{Q}}(s)$ and $\tilde{\mathbf{R}}(s)$, as required by Algorithm II. The corresponding analysis for the interpolation of $\tilde{\mathbf{q}}_k(s)$ and $\tilde{\mathbf{r}}_k^T(s)$, $k = 1, 2, \dots, M_T$, as required by Algorithm III, is more involved and does not yield any additional insight into the trade-off under consideration. The numerical results presented in the following demonstrate that for Algorithm II to have smaller complexity than Algorithm I, setting B' to a value smaller than $V + 1$, and hence accepting a systematic interpolation error, may be necessary. On the other hand, we will also see that the resulting performance degradation, in terms of both coded and uncoded bit error rate (BER), can be negligible even for values of B' that are significantly smaller than $V + 1$.

In the following, we consider a MIMO-OFDM system with $D = N = 512$, $M_R = 4$, and either $M_T = 2$ or $M_T = 4$, operating over a frequency-selective channel with $L = 15$. The data symbols are drawn from a 16-QAM constellation. In the coded case, a rate 1/2 convolutional code with constraint length 7 and generator polynomials [133_o 171_o] is used. The receiver performs maximum-likelihood detection through hard-output sphere decoding. Our results are obtained through Monte Carlo simulation, where averaging is performed over the channel impulse response taps $\mathbf{H}_0, \mathbf{H}_1, \dots, \mathbf{H}_L$ assumed i.i.d. $\mathcal{CN}(0, 1/(L + 1))$. This assumption on the channel statistics, along with the average transmit power being given by $\mathbb{E}[\mathbf{c}_n^H \mathbf{c}_n] = 1$ and the noise variance σ_w^2 , implies that the per-antenna receive signal-to-noise ratio (SNR) is $1/\sigma_w^2$. The receiver employs either Algorithm I or Algorithm II to compute $\mathbf{Q}(s_n)$ and $\mathbf{R}(s_n)$ at all tones. We assume that in Step 1 of both algorithms, $\mathbf{H}(s) \sim (0, L)$ is interpolated exactly from $B = L + 1 = 16$ equidistant base points by FIR filtering. Since $0 = V_1 \neq V_2 = L$, the corresponding interpolation complexity per target point is obtained from (62) as $c_{\text{IP}, \mathbf{H}} \triangleq (L + 1)\chi_{\mathbb{C}}/2$. With $\chi_{\mathbb{C}} = 1/4$, as assumed in Section 8.1, we get⁸ $c_{\text{IP}, \mathbf{H}} = 2$. In Step 4 of Algorithm II, we interpolate $\tilde{\mathbf{Q}}(s) \sim (M_T L, M_T L)$ and $\tilde{\mathbf{R}}(s) \sim (M_T L, M_T L)$, with maximum degree $V = 2M_T L$, through FIR filtering from $B' \leq B = 2^{\lceil \log(V+1) \rceil}$ base points. With $V_1 = V_2 = M_T L$, the corresponding interpolation complexity per target point is obtained from (64) as $c_{\text{IP}, \tilde{\mathbf{Q}}\tilde{\mathbf{R}}} \triangleq \chi_{\mathbb{R}} B'/2$ with $\chi_{\mathbb{R}} = 1/8$, as assumed in Section 8.1. We ensure that systematic interpolation errors are the sole source of detection performance degradation by performing all computations in double-precision floating-point arithmetic. Under inexact interpolation, for every value of $B' < V + 1$ we determine the value of V'_1 that minimizes the interpolation error $e(\mathbf{F}_0)$ in (65) according to the procedure described in Section 8.5.

⁸Performing interpolation of $\mathbf{H}(s)$ by FFT would lead to $c_{\text{IP}, \mathbf{H}}$ according to (59), which with $B = 16$ and $R = N/B = 32$ results in $c_{\text{IP}, \mathbf{H}} = 64/31 \approx 2.06$. Hence, in this case interpolation of $\mathbf{H}(s)$ by FIR filtering and by FFT have comparable complexity.

Table 2: Simulation parameters

M_T	B'	V'_1	$c_{\text{IP},\tilde{\mathbf{Q}}\tilde{\mathbf{R}}}$	$C_{\text{II}}/C_{\text{I}}$	Interpolation method
2	64	30	3.43	0.74	FFT, exact
2	64	30	4	0.82	FIR filtering, exact
2	32	27	2	0.55	FIR filtering, inexact
2	16	25	1	0.41	FIR filtering, inexact
2	12	23	0.75	0.37	FIR filtering, inexact
2	8	21	0.5	0.34	FIR filtering, inexact
4	128	60	4.67	1.08	FFT, exact
4	128	60	8	1.54	FIR filtering, exact
4	32	50	2	0.71	FIR filtering, inexact
4	24	48	1.5	0.64	FIR filtering, inexact
4	16	42	1	0.57	FIR filtering, inexact
4	8	31	0.5	0.50	FIR filtering, inexact

Common to all simulations are the parameters $D = N = 512$, $L = 15$, $M_R = 4$, and $c_{\text{IP},\mathbf{H}} = 2$.

Table 2 summarizes the simulation parameters, along with the corresponding values of the interpolation complexity per target point $c_{\text{IP},\tilde{\mathbf{Q}}\tilde{\mathbf{R}}}$ and the resulting algorithm complexity ratio $C_{\text{II}}/C_{\text{I}}$, which quantifies the savings of Algorithm II over Algorithm I. The values of $C_{\text{II}}/C_{\text{I}}$ for the case where $\tilde{\mathbf{Q}}(s)$ and $\tilde{\mathbf{R}}(s)$ are interpolated exactly by FFT are provided for reference. We note that for $M_T = 4$, exact interpolation, both FFT-based and through FIR filtering, results in $C_{\text{II}} > C_{\text{I}}$. Hence, in this case inexact interpolation is necessary to obtain complexity savings of Algorithm II over Algorithm I. In contrast, for $M_T = 2$, Algorithm II exhibits lower complexity than Algorithm I even in the case of exact interpolation.

Figs. 3a and 3b show the resulting BER performance for $M_T = 2$ and $M_T = 4$, respectively, both for the coded and the uncoded case. For uncoded transmission and inexact interpolation, we observe an error floor at high SNR which rises with decreasing B' . For $M_T = 2$ and uncoded transmission, we can see in Fig. 3a and Table 2, respectively, that an interpolation filter length of $B' = 8$ results in negligible performance loss for SNR values of up to 18 dB, and yields complexity savings of Algorithm II over Algorithm I of 66%. Choosing $B' = 16$ yields close-to-optimum performance for SNR values of up to 24 dB and complexity savings of 59%. For $M_T = 4$ and uncoded transmission, Fig. 3b and Table 2 show that the interpolation filter length can be shortened from $B' = 128$ to $B' = 8$, leading to complexity savings of Algorithm II over Algorithm I of 50%, at virtually no performance loss in the SNR range of up to 21 dB. Setting $B' = 32$ results in a performance loss, compared to exact interpolation, of less than 1 dB at $\text{BER} = 10^{-6}$ and in complexity savings of 29%. In the coded case, both for $M_T = 2$ and $M_T = 4$, we can see in Figs. 3a and 3b that the BER curves for Algorithm II, for all values of B' under consideration, essentially overlap with the

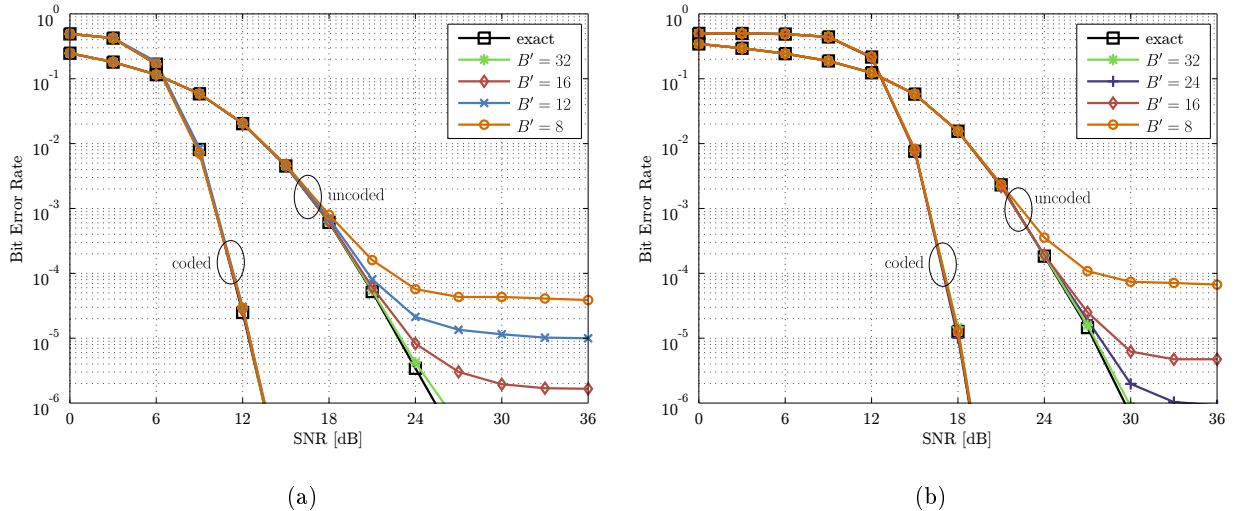


Figure 3: Bit error rates as a function of SNR for different interpolation filter lengths, with and without channel coding, for (a) $M_T = 2$ and (b) $M_T = 4$. The results corresponding to exact QR decomposition are provided for reference.

corresponding curves for Algorithm I for BERs down to 10^{-6} . This observation suggests that for a given target BER and a given tolerated performance loss of Algorithm II over Algorithm I, the use of channel coding allows to employ significantly shorter interpolation filters (corresponding to a smaller $c_{\text{IP},\tilde{\mathbf{Q}}\tilde{\mathbf{R}}}$ and hence to a lower C_{II} , which in turn implies higher savings of Algorithm II over Algorithm I) than in the uncoded case. We conclude that in the practically relevant case of coded transmission, complexity savings of Algorithm II over Algorithm I can be obtained at negligible detection performance loss.

9.2. Algorithm Complexity Comparisons

The discussion in Section 8 and the numerical results in Section 9.1 demonstrated that for the case of upsampling from equidistant base points, small values of c_{IP} can be achieved and inexact interpolation does not necessarily induce a significant detection performance loss. Therefore, in the following we assume that for all $k = 1, 2, \dots, M_T$, the set \mathcal{I}_k is such that $\mathcal{S}(\mathcal{I}_k)$ contains $B_k = |\mathcal{I}_k| = 2^{\lceil \log_2(2kL+1) \rceil}$ base points that are equidistant on \mathcal{U} , and assume that $c_{\text{IP}} = 2$. The latter assumption is in line with the values of $c_{\text{IP},\mathbf{H}}$ and $c_{\text{IP},\tilde{\mathbf{Q}}\tilde{\mathbf{R}}}$ found in Section 9.1.

For $D = 500$, $L = 15$, and different values of M_T and M_R , Fig. 4a shows the complexity of Algorithms II and III as percentage of the complexity of Algorithm I. We observe savings of Algorithms II and III over Algorithm I as high as 48% and 62%, respectively. Furthermore, we can see that Algorithm III exhibits a lower complexity than Algorithm II in all considered configurations. We note that the latter behavior is a consequence of the small value of c_{IP} and of Algorithm III, with respect to Algorithm II, trading a lower QR decomposition cost against a higher interpolation cost. Moreover, we observe that the savings of Algorithms II and III over Algorithm I are more pronounced for larger $M_R - M_T$. For the special case

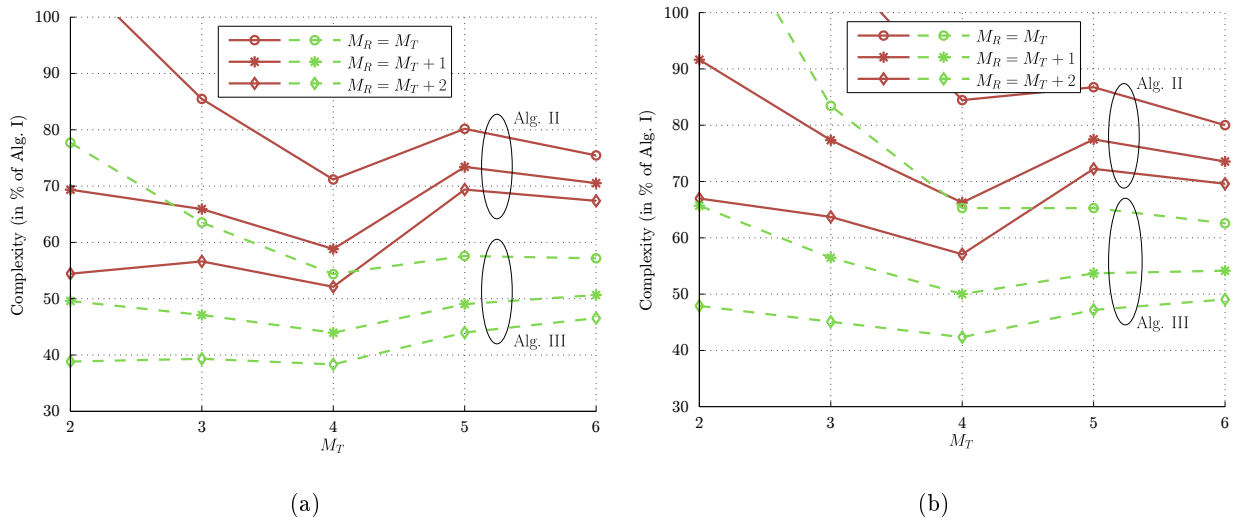


Figure 4: Complexity of Algorithms II and III as percentage of complexity of Algorithm I for $D = 500$, and $L = 15$, (a) including and (b) excluding the complexity of interpolation of $\mathbf{H}(s)$.

$\mathcal{E} = \mathcal{D}$, where interpolation of $\mathbf{H}(s)$ is not necessary and Algorithm I simplifies to the computation of D QR decompositions, Fig. 4b shows that the relative savings of Algorithms II and III over Algorithm I are somewhat reduced, but still significant. We can therefore conclude that interpolation-based QR decomposition, provided that the complexity of interpolation is sufficiently small, yields fundamental complexity savings.

For $D = 500$, $M_T = M_R$, and different values of L , Fig. 5a shows the complexity of Algorithms II-MMSE and III-MMSE as percentage of the complexity of Algorithm I-MMSE. The fact (which also carries over to the savings of Algorithms II and III over Algorithm I) that the savings of Algorithms II-MMSE and III-MMSE over Algorithm I-MMSE are more pronounced for smaller values of L is a consequence of B_k being an increasing function of L . In Fig. 5a, we can see that despite the low interpolation complexity implied by $c_{IP} = 2$, Algorithm III-MMSE may exhibit a higher complexity than Algorithm II-MMSE. This is a consequence of the fact that for some values of M_T , M_R , and L , the overall complexity of the UT-based QR decompositions with standard form (49) required in Algorithm III-MMSE is larger than the overall complexity of the efficient UT-based regularized MMSE-QR decompositions with standard form (51) required in Algorithm II-MMSE.

Finally, Fig. 5b shows the absolute complexity of Algorithms I–III and I-MMSE through III-MMSE as a function of D , for $M_T = 3$, $M_R = 4$, and $L = 15$. We observe that the complexity savings of Algorithms II and III over Algorithm I and the savings of Algorithms II-MMSE and III-MMSE over Algorithm I-MMSE grow linearly in D . This behavior was predicted for Algorithms I and II by the analysis in Section 6.4, where we showed that $C_I - C_{II}$ is an affine function of D and is positive for small c_{IP} and large D .

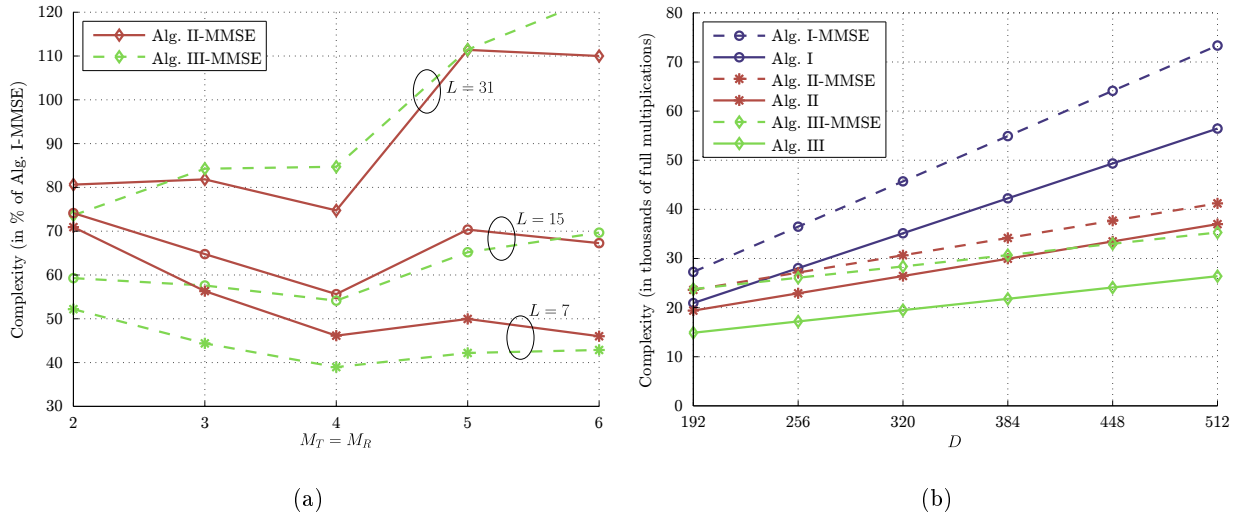


Figure 5: (a) Complexity of Algorithms II-MMSE and III-MMSE as percentage of complexity of Algorithm I-MMSE for $D = 500$ and $L = 15$. (b) Absolute complexity of Algorithms I-III and I-MMSE through III-MMSE, for $M_T = 3$, $M_R = 4$, and $L = 15$.

10. Conclusions and Outlook

On the basis of a new result on the QR decomposition of LP matrices, we formulated interpolation-based algorithms for computationally efficient QR decomposition of polynomial matrices that are oversampled on the unit circle. These algorithms are of practical relevance as they allow for an (often drastic) reduction of the receiver complexity in MIMO-OFDM systems. Using a complexity metric relevant for VLSI implementations, we demonstrated significant and fundamental complexity savings of the proposed new class of algorithms over brute-force per-tone QR decomposition. The savings are more pronounced for larger numbers of data-carrying tones and smaller channel orders. We furthermore provided strategies for low-complexity interpolation exploiting the specific structure of the problem at hand.

The fact that the maximum degree of the LP matrices $\tilde{\mathbf{Q}}(s)$ and $\tilde{\mathbf{R}}(s)$ is $2M_T L$, although the polynomial MIMO transfer function matrix $\mathbf{H}(s)$ has maximum degree L , gives rise to the following open questions:

- Is the mapping \mathcal{M} optimal in the sense of delivering LP matrices with the lowest maximum degree?
- Would interpolation-based algorithms for QR decomposition that explicitly make use of the unitarity of $\mathbf{Q}(s)$ allow to further reduce the number of base points required and hence lead to further complexity savings?

Additional challenges include the extension of the ideas presented in this paper to sparse channel impulse responses, for which only few of the impulse response tap matrices are nonzero.

Acknowledgments

The authors would like to thank Andreas Burg and Simon Haene for many inspiring and helpful discussions, Jan Hansen and Moritz Borgmann for their contributions in early stages of this work, and Gerhard Doblinger for bringing [15] to their attention.

References

- [1] M. Borgmann, H. Bölcskei, Interpolation-based efficient matrix inversion for MIMO-OFDM receivers, in: Proc. Asilomar Conf. Signals, Syst., Comput., Pacific Grove, CA, 2004, pp. 1941–1947.
- [2] E. O. Brigham, The Fast Fourier Transform, Prentice Hall, Englewood Cliffs, NJ, 1974.
- [3] A. Burg, VLSI Circuits for MIMO Communication Systems, vol. 169 of Series in Microelectronics, Hartung-Gorre, Konstanz, Germany, 2006, Ph.D. thesis, ETH Zurich.
- [4] L. M. Davis, Scaled and decoupled Cholesky and QR decompositions with application to spherical MIMO detection, in: Proc. IEEE Wireless Commun. Netw. Conf. (WCNC), New Orleans, LA, 2003, pp. 326–331.
- [5] U. Fincke, M. Pohst, Improved methods for calculating vectors of short length in a lattice, including a complexity analysis, *Math. Comp.* 44 (170) (1985) 463–471.
- [6] G. H. Golub, C. F. Van Loan, Matrix Computations, 3rd ed., Johns Hopkins Univ. Press, Baltimore, MD, 1996.
- [7] S. Haene, A. Burg, N. Felber, W. Fichtner, OFDM channel estimation algorithm and ASIC implementation, in: Proc. IEEE Int. Conf. Circuits and Syst. Commun. (ICCSC), Bucharest, Romania, 2006, pp. 270–275.
- [8] B. Hassibi, An efficient square-root algorithm for BLAST, in: Proc. IEEE Int. Conf. Acoust., Speech, Signal Process. (ICASSP), vol. 2, Istanbul, Turkey, 2000, pp. 737–740.
- [9] R. A. Horn, C. R. Johnson, Matrix Analysis, Cambridge Univ. Press, Cambridge, U.K., 1985.
- [10] H. Kaeslin, Digital Integrated Circuit Design, Cambridge Univ. Press, Cambridge, U.K., 2008.
- [11] V. Lefèvre, Multiplication by an integer constant, Tech. Rep. RR-4192, INRIA (May 2001).
- [12] G. Lightbody, R. Woods, R. Walke, Design of a parameterizable silicon intellectual property core for QR-based RLS filtering, *IEEE Trans. VLSI Syst.* 11 (2003) 659–678.
- [13] A. J. Paulraj, R. U. Nabar, D. A. Gore, Introduction to Space-Time Wireless Communications, Cambridge Univ. Press, Cambridge, U.K., 2003.
- [14] D. Perels, S. Haene, P. Luethi, A. Burg, N. Felber, W. Fichtner, H. Bölcskei, ASIC implementation of a MIMO-OFDM transceiver for 192 Mbps WLANs, in: Proc. IEEE Eur. Solid-State Circuits Conf. (ESSCIRC), Grenoble, France, 2005, pp. 215–218.
- [15] D. P. Skinner, Pruning the decimation-in-time FFT algorithm, *IEEE Trans. Acoust., Speech, Signal Process.* 24 (2) (1976) 193–194.
- [16] C. Studer, A. Burg, H. Bölcskei, Soft-output sphere decoding: Algorithms and VLSI implementation, *IEEE J. Sel. Areas Commun.* 26 (2) (2008) 290–300.
- [17] E. Viterbo, E. Biglieri, A universal decoding algorithm for lattice codes, in: Proc. GRETSI Symp. Signal and Image Process., Juan-les-Pins, France, 1993, pp. 611–614.
- [18] J. Volder, The CORDIC trigonometric computing technique, *IRE Trans. Electron. Comput.* EC-8 (3) (1959) 330–334.
- [19] J. S. Walther, The story of unified CORDIC, *Kluwer J. VLSI Signal Process.* 25 (2000) 107–112.
- [20] C. Windpassinger, R. F. H. Fischer, T. Vencel, J. B. Huber, Precoding in multi-antenna and multi-user communication, *IEEE Trans. Wireless Commun.* 3 (4) (2004) 1305–1316.

- [21] P. Wolniansky, G. Foschini, G. Golden, R. Valenzuela, VBLAST: An architecture for realizing very high data rates over the rich-scattering wireless channel, in: Proc. URSI Symp. Signals, Syst., Electron. (ISSSE), Pisa, Italy, 1998, pp. 295–300.
- [22] D. Wübben, K.-D. Kammeyer, Interpolation-based successive interference cancellation for per-antenna-coded MIMO-OFDM systems using P-SQRD, in: Proc. IEEE Workshop Smart Antennas, Ulm, Germany, 2006.